AD NUMBER

AD476001

LIMITATION CHANGES

TO:

Approved for public release; distribution is unlimited.

FROM:

**Distribution authorized to U.S. Gov't. agencies and their contractors;
Administrative/Operational Use; 29 NOV 1965.
Other requests shall be referred to Office of Naval Research, Arlington, VA 22203.**

AUTHORITY

ONR ltr 27 Jul 1971

OPTICAL SPECTROSCOPY AND CRYSTAL GROWTH OF CeO_2 AND ThO_2

YEARLY TECHNICAL SUMMARY REPORT

(For the Period Ending 31 October 1965)

Contract No. Nonr 4660(00)
ARPA Order No. 306-62
Project Code No. 4730

Perkin-Elmer Engineering Report No. 8197

Robert C. Linares
Principal Investigator

 This research is part of Project DEFENDER under the joint sponsorship of the Advanced Research Project Agency, the Office of Naval Research and the Department of Defense.

The Perkin-Elmer Corporation
Electro-Optical Division
Norwalk, Connecticut 06852

TABLE OF CONTENTS

LIST OF TABLES

LIST OF ILLUSTRATIONS

LIST OF ILLUSTRATIONS (Continued)

The Perkin-Elmer Corporation
Electro-Optical Division

Report No. 8197

ABSTRACT

The crystal growth and optical spectra of CeO_2 and ThO_2 were studied to determine their potential usefulness as laser materials. Crystal growth was carried out by the flux technique. Phase equilibria and solubility determinations were made in order to develop a flux for the eventual growth of laser-size crystals.

The trivalent rare earths, tetravalent niobium and uranium and some nobel metal ions were incorporated into single crystals of CeO_2 and ThO_2. Transmission measurements were made throughout the wavelength region between 2000Å and 100,000Å. When samples were observed to fluoresce with X-ray, UV or visible excitation, their emission spectra, excitation spectra, and fluorescent lifetime were studied. The effect of charge compensation on these properties was also studied.

SECTION I

INTRODUCTION

Cerium dioxide and thorium dioxide crystallize in the fluorite structure with lattice constants of 5.411Å and 5.600Å respectively. The ionic radius of Ce^{4+} is 0.96Å and that of Th^{4+} is 1.04Å, making the substitution of all the rare earths possible. In the fluorite structure, the cations occupy a site of high symmetry, substitution into which was hoped to give a phosphor with a long fluorescent lifetime. However, if the substituted fluorescent ion is not tetravalent, the type of charge compensation will determine the site symmetry.

Studies made on Er^{3+} and Yb^{3+} in ThO_2 using ESR[1] have shown that the rare earth can occupy both cubic and trigonal sites. The cubic predominates at low rare earth concentration and the trigonal at high concentrations. This observation can be explained on the basis of the increased probability that a charge compensating hole will reside near a rare earth ion. The same situation may be expected to occur in CeO_2. It so, it should be possible to prepare these crystals with the rare earth in the two difference sites and study the effect of site symmetry on the optical emission. Further, it should be possible to change the number of ions in a site by varying amount and type of a charge compensation ion.

Charge compensation of a trivalent ion in CeO_2 or ThO_2 can be accomplished most easily by the following mechanisms:

$$2Me^{+4} + 4O^{-2} = 2Re^{+3} + 3O^{-2} + 0 \text{ vacancy}$$

$$2Me^{+4} + 4O^{-2} = Re^{+3} + Nb, Ta^{+5} + 4O^{-2}$$

$$Me^{+4} + 2O^{-2} = Re^{+3} + O^{-2} + F^{-1}$$

Charge compensation of a divalent ion can be accomplished by the following mechanisms:

$$2Me^{+4} + 4O^{-2} = Re^{+2} + W, Mo^{+6} + 4O^{-2}$$

$$3Me^{+4} + 6O^{-2} = Re^{+2} + 2Nb, Ta^{+5} + 6O^{-2}$$

$$Me^{+4} + 2O^{-2} = Re^{+2} + 2F^{-1}$$

It is evident that these mechanisms will be unsuitable at high concentrations because they will destroy the cubic symmetry around the ion. Even at low concentrations, cubic site symmetry will not be attained unless the compensating center is beyond the Coulomb field of the dopant. Further, since optical studies of Gd^{3+} and U^{3+} in CaF_2 indicate there are many more than two sites for a trivalent ion in this compound,[2] we may expect more than two sites to be observed ThO_2 or CeO_2.

1. Experimental Program

The experimental program was divided into two areas, crystal growth and measurements. The crystal growth experiments were confined to the flux technique. The phase equilibrium and solubilities were explored. During the first period of work, experiments were mainly conducted on CeO_2. However, it became apparent that ThO_2 had many important advantages over CeO_2, and the emphasis was shifted to ThO_2 during the second period of work. The measurements made were

emission spectra, transmission, fluorescent lifetime and excitation spectra. So that emphasis could be placed on the growth of large crystals, work on hydrothermal equilibria was not performed, as forecast in the Semiannual Report.

SECTION II

FLUX GROWTH OF CeO_2 AND ThO_2

Because of the extremely high melting points of CeO_2 and ThO_2 (2800°C and 3800°C respectively), the flux technique is most attractive for the growth of these crystals. While a number of fluxes have been reported recently for the growth of ThO_2[3], there was a complete void in the literature about the growth of crystals of CeO_2 and ThO_2 at the beginning of this program. To make these materials available for study, the phase equilibria, solubilities, crystal morphology and crystal growth in various molten salts were explored.

1. Phase Equilibria

The phase equilibrium runs were made by cooling a melt of flux saturated with CeO_2 or ThO_2 from 1300°C to 900°C at 5° per hour. The identity of the crystallized phase was determined by X-ray diffraction or microscopic inspection. On the basis of melting points and volatility of fluxes and temperature limitations of the furnaces, the temperature range explored was from 1350°C to 900°C.

a. Cerium Oxide

A large number of fluxes were tried for CeO_2. Of these systems, three appeared promising and were explored in detail. These systems are:

1. $PbO - PbF_2 - B_2O_3$
2. $Li_2O - MoO_3 - B_2O_3$
3. $Na_2O - MoO_3 - B_2O_3$

Details of explorations of these systems and their solubilities are given in Appendix I.

b. Thorium Oxide

Thorium oxide was found to be stable with roughly the same flux compositions as CeO_2 in the Na_2O-B_2O_3 and PbO-PbF_2-B_2O_3 systems. In addition, the ternary NaF-PbF_2-B_2O_3 was explored for the growth of ThO_2. Here, ThO_2 was stable with as little as ~ 50 mole percent PbF_2 or up to ~ 80 mole percent NaF. A flux containing 75 mole percent PbF_2, 16.7 mole percent NaF and 8.3 mole percent B_2O_3 was optimum for lead-containing fluxes. A flux containing 66.6 mole percent NaF and 33.3 mole percent B_2O_3 was optimum for the lead-free fluxes.

2. Growth Morphology

Crystal growth was accomplished by slow cooling of the flux saturated with CeO_2 or ThO_2 at 1 to 5°C/hr. In these experiments, two morphologies were found. One is a cube bonded by $\{100\}$ faces and the other an octahedron bonded by $\{111\}$ faces.

The cube form is usually characterized by large regions of lamellar growth (Figure 1) with flux included between the lamellae. The octahedral form (Figure 2) shows no lamellar growth and usually has very large areas free of flux inclusions. Some relatively perfect cubes of CeO_2 have been formed, but are of a much smaller percentage yield than the octahedra. However, with the lead fluxes, ThO_2 cubes can form which are entirely free of lamellae (Figure 3).

A list of the fluxes and the morphologies of CeO_2 yielded are given in Table I. Octahedra are only obtained from: (1) the $Na_2O \cdot B_2O_3$ system when

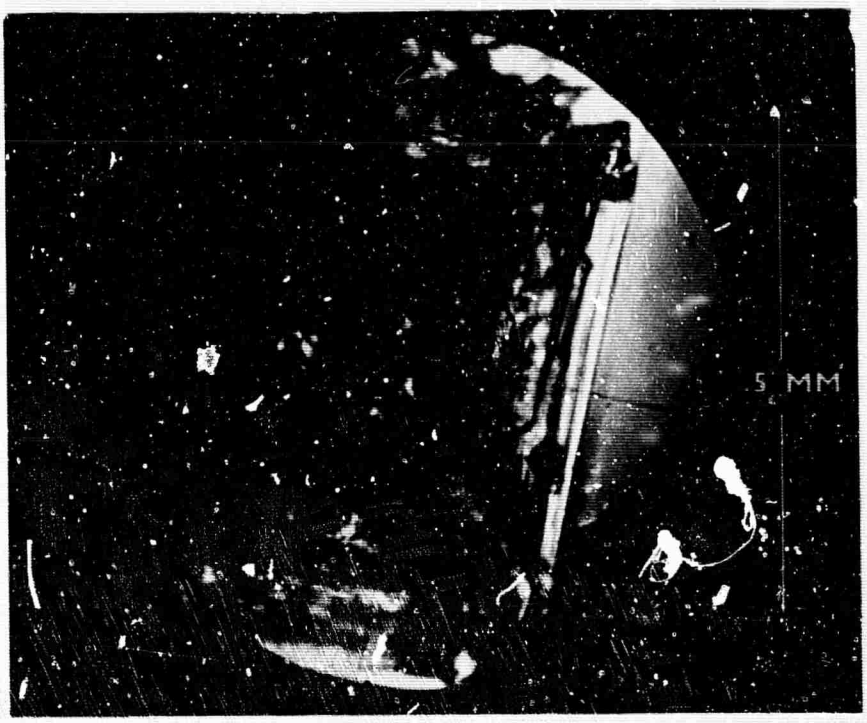

Figure 1. CeO_2 Cube

Figure 2. CeO_2 Octahedra

Na/B ≥ 1.0 and (2) the $Li_2O \cdot B_2O_3 \cdot MoO_3$ system when Mo/B ≥ 1.0. The controlling influence of the information of octahedra is the sodium or the molybdenum content of the flux.

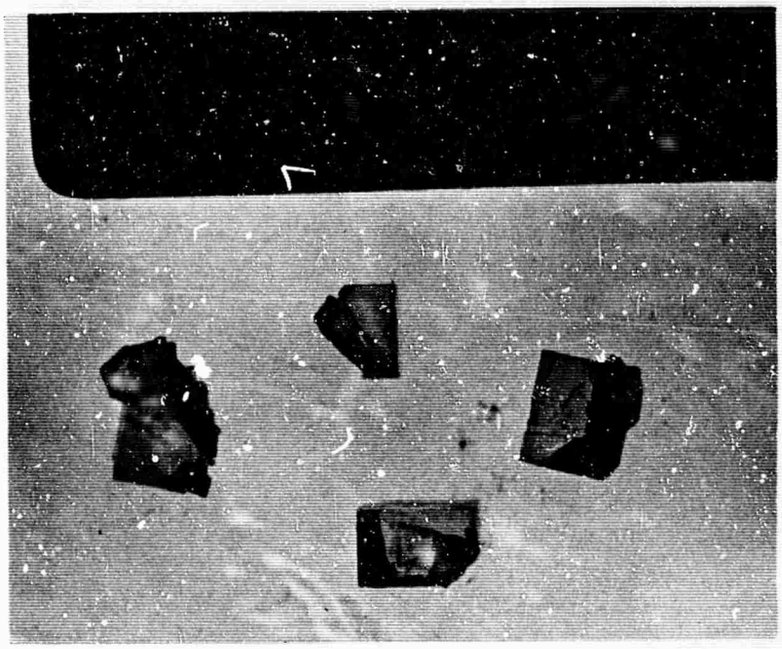

Figure 3. ThO_2 Cubes

Mixtures of lead fluxes and $NaBO_2$ were made in the hope that a flux of relatively high solubility could be found which would yield octahedra. It was found that the transition from cubes to octahedra could not be mad' in such mixtures without too great a decrease in solubility. The transition between cubes and octahedra does not occur suddenly, but goes through a region of dendritic growth. The dendritic growth (Figure 4) has the appearance of cubes stacked on their corners. This condition persists over flux compositions 0.8 to 0.7 $NaBO_2$ · 0.2 to 0.3 PbF_2. Outside this flux componsition only octahedra or cubes are found.

TABLE I

MORPHOLOGY OF CeO_2 WITH VARIOUS FLUXES

Flux Composition	Morphology
10 $PbO \cdot B_2O_3$	Cubes
10 $PbF_2 \cdot B_2O_3$	Cubes
$PbO \cdot PbF_2$	Cubes
$Li_2O \cdot B_2O_3$	Cubes
$Li_2O \cdot 2B_2O_3$	Cubes
$Na_2O \cdot 2B_2O_3$	Cubes
$Na_2O \cdot B_2O_3$	Octahedra
$Li_2O \cdot 2MoO_3$	Octahedra
$Li_2O \cdot 4MoO_3$	Octahedra
$Li_2O \cdot B_2O_3 \cdot MoO_3$	Cubes & Octahedra
$Li_2O \cdot 1/2\ B_2O_3 \cdot 3MoO_3$	Octahedra
$Li_2O \cdot 1\ 1/2\ B_2O_3 \cdot MoO_3$	Cubes

Figure 4. Dendritic CeO_2

The morphology of ThO_2 was found to vary with changes of flux in exactly the same manner as the CeO_2, except that in the $NaF-PbF_2-B_2O_3$ system, ThO_2 octahedra were not formed in the ThO_2 stability region.

3. Growth of Large Crystals

a. Slow Cooling of CeO_2

A large number of small crystal growth runs (100 ml crucible) were made by using flux compositions according to the solubility curves shown in Appendix I and slowly (0.75° to 1.0°/hour) cooling over the range (1300° to 900°C). The flux compositions were chosen as being representative of the different flux systems and morphology variations. It was found that on the basis

of growth rate and perfection, only the $NaBO_2$, $Li_2Mo_2O_7$, and PbF_2-x B_2O_3 compositions had potential for the growth of large crystals.

A scale-up of the process to a 2000 ml container was made, using these three fluxes. Cooling rates of 1°/hour were used to keep the runs to a reasonable length of time.

Using the $NaBO_2$ flux, clear octahedral crystals were obtained that were no larger than 1 mm on an edge. It was found that going to these slow rates actually resulted in poorer quality crystals. It is believed that this was caused by a loss of Na_2O from the melt by evaporation over a period of one to two weeks, which pushes the melt composition toward the stability region for cubes. This hypothesis is substantiated by the appearance of small $\{100\}$ faces on the octahedra.

Using the PbF_2-B_2O_3 flux, crystals 3 mm on an edge have been obtained. These crystals were of very poor optical quality and contain color centers which have been traced to the incorporation of Ca^{2+}, Pb^{2+} and F^{1-} into the crystals. This is discussed in detail under the section entitled "Transmission".

Slow cooling of large Li_2O-MoO_3-CeO_2 melts did not yield large crystals because spontaneous nucleation is common in this system.

b. Slow Cooling of ThO_2

Unlike CeO_2, ThO_2 has little or no color center formation from Ca^{2+} and F^{1-} and yields cubes that are relatively lamellae-free from PbF_2-B_2O_3 mixtures. Experiments with PbF_2-B_2O_3-NaF systems showed that flux compositions of 75 mole percent PbF_2, 16.7 mole percent NaF and 8.3 mole percent B_2O_3 produced

crystals three times the size of those obtained from PbF_2 alone. In runs cooled from 1300°C at 0.5°/hour for one week and at 1°/hour at temperatures to 1000°C, clear crystals have been obtained which permitted fabrication of rods 1/2-inch long by 1/8-inch diameter for laser testing.

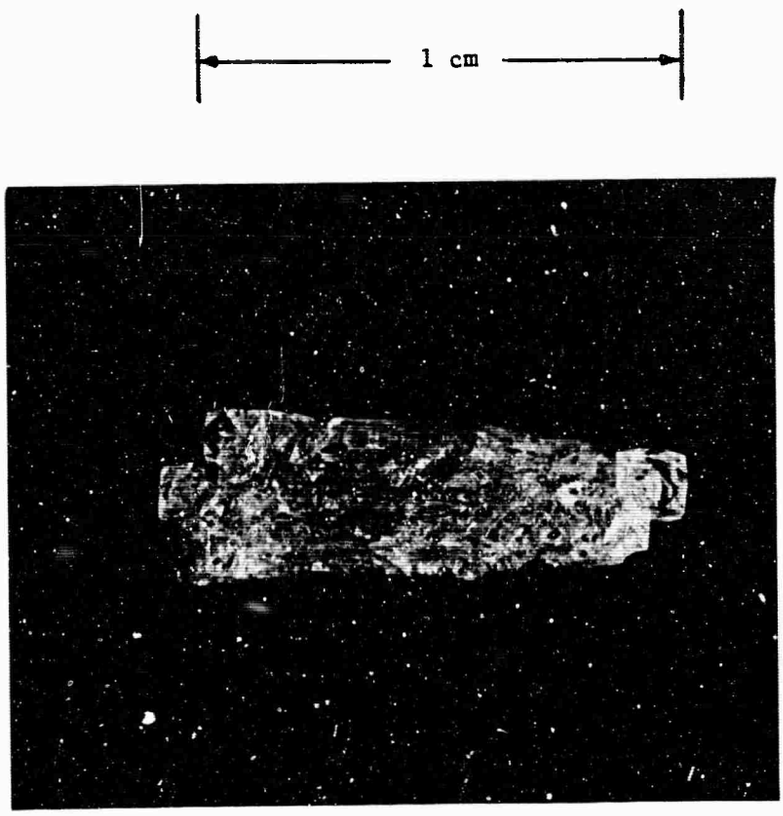

Figure 5. Seeded ThO_2

ThO_2 crystals grown from lead fluxes exhibit UV damage. Therefore, experiments were conducted to use ThO_2 crystals from a lead flux as seeds for growth from lead-free fluxes. The procedure followed was to first make a solution of $NaBO_2$ or $2NaF\text{-}B_2O_3$, saturated with ThO_2 at 1300°C. Then a seed of ThO_2 is introduced and cooling is begun. The run is terminated by pouring the flux off and cooling slowly to room temperature. Using cooling rates of 2°/hour stepped crystals grow (Figure 5) which have sections of good optical quality.

These crystals were somewhat dissolved prior to growth and there was considerable spontaneous nucleation on the crucible walls. If these two problems are controlled properly, by closer regulation of the chemical composition and slower cooling, large lead-free crystals can be grown.

c. Gradient Growth

In the gradient method[4], a seed crystal is hung in the cooler, top region of a crucible and nutrient is placed in the cooler, bottom region of the crucible (Figure 6). Growth occurs by dissolution of the nutrient and deposition on the seed.

Gradient growth of CeO_2 was accomplished using $Li_2Mo_2O_7$ flux, which gives octahedral growth. Since octahedral growth is characterized by rapid growth of the $\{100\}$ faces, it was thought advantageous to use cubes as seeds, to obtain maximum growth. This is not desirable, because even with very small ΔT between growth region and nutrient, growth occurred rapidly and resulted in poor quality (Figure 7). Using an octahedral seed crystal, high-quality growth occurs slowly.

In experiments aimed at optimizing growth rate and crystal quality, the ΔT and growth temperature were varied independently. It was found that growth rate did increase linearly with ΔT; unfortunately, spontaneous nucleation at the surface of the liquid also became an increasing problem. Growth temperatures of 970°C and ΔT of 100° were the maximum tolerable. This gave a growth rate of 0.25 mm/day and high quality growth as shown in Figure 8. With large seeds it would be possible to grow large CeO_2 crystals by this method.

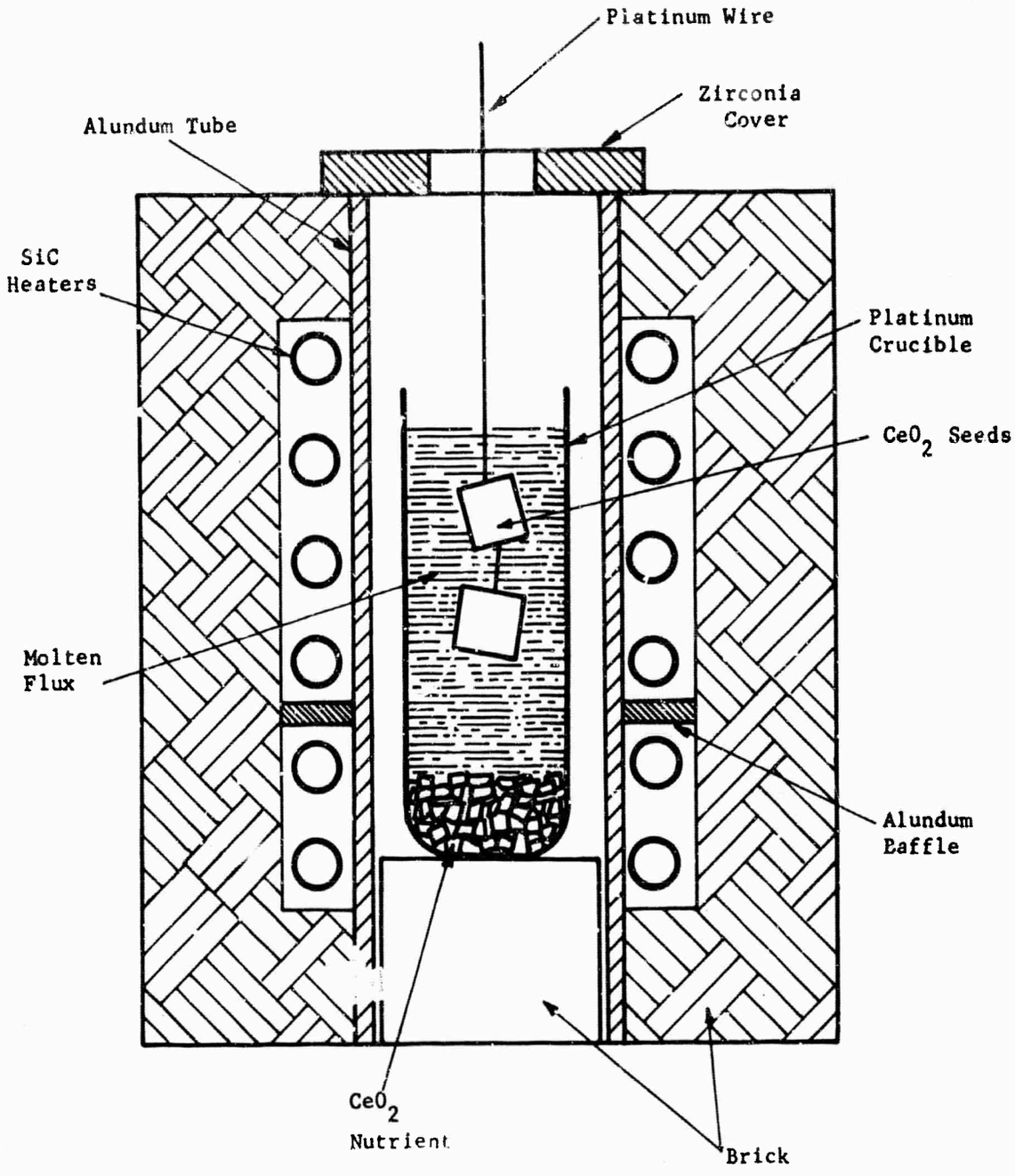

Figure 6. Gradient Flux Growth Apparatus

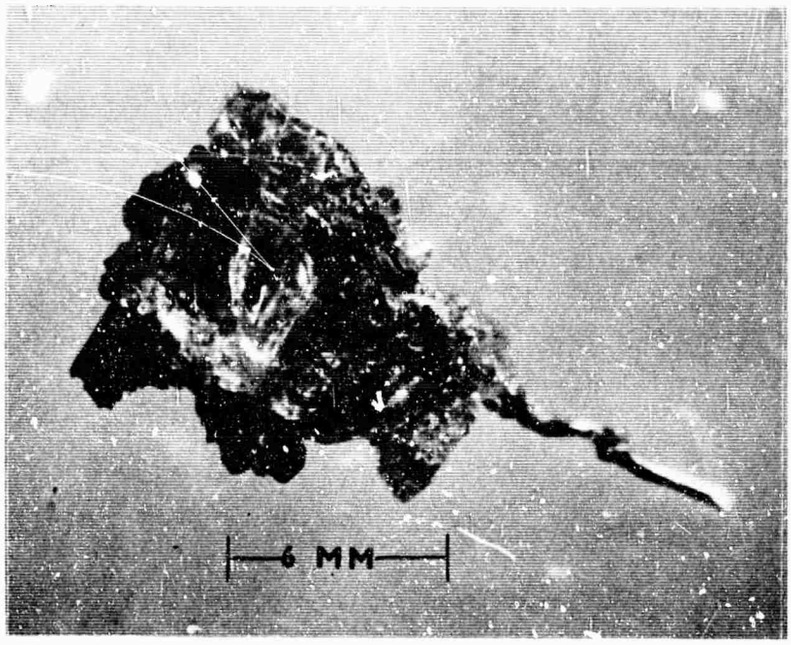

Figure 7. Gradient-Grown Octahedral CeO_2 on Cubic Seed

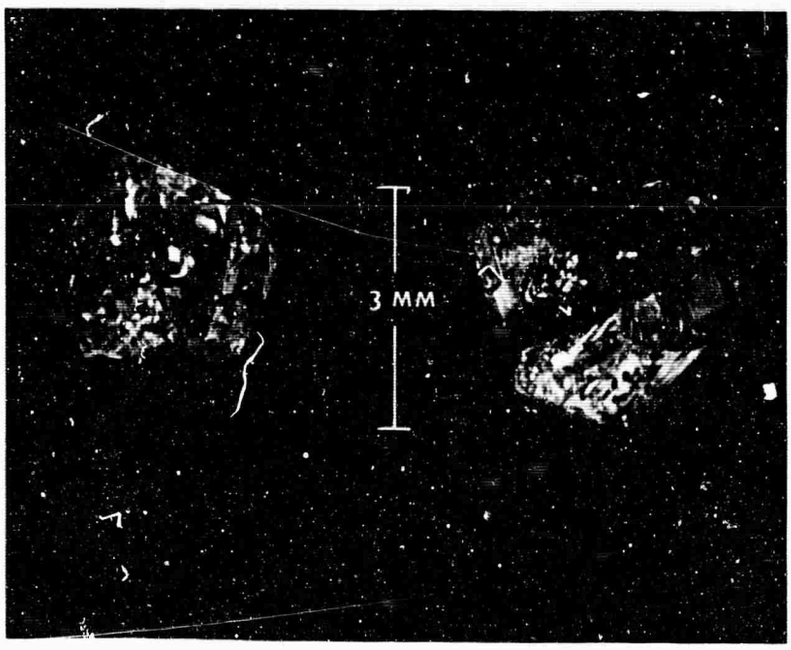

Figure 8. Gradient-Grown CeO_2

A few gradient runs with ThO_2 were made using $NaBO_2$ flux. Growth conditions of 1027°C deposition temperature with a 25° ΔT resulted in growth of less than 0.025 mm/day. Much more work is required in this area to give suitable results.

SECTION III

MEASUREMENTS

1. Experimental Measurements

Visible emission spectra were excited by X-rays. This technique was demonstrated by Low[5] and was successfully applied to rare earth spectroscopy in our laboratory (Appendix II). This experimental setup was used to measure the visible emission spectra. The infrared emission spectra were excited by a 1 kw quartz iodine lamp. In both cases the spectra were measured using a 0.58 Meter Ebert Grating Monochromator (Perkin-Elmer Model 231). The instrument was operated with an over-and-under, double-pass arrangement to reduce scattered light. A 1400 line/mm and 576 line/mm grating were used for the visible and infrared, respectively. This allowed first-order scanning from 3700Å to 25000Å. The resolution of the instrument is better than 0.1Å in the visible region.

Four different types of detectors were used to give greater efficiency over the wavelength range used. These were:

3700Å	to	7000Å	-	Hand-selected, red-sensitive EMI 6705 photomultiplier (S-10 surface)
7000Å	to	9000Å	-	RCA 7102 photomultiplier (S-1 surface)
9000Å	to	12000Å	-	RCA EJ-2471 Lithium drifted diode
12000Å	to	25000Å	-	Perkin-Elmer lead sulfide cell

Transmission measurements were made with a Perkin-Elmer Model 450 or Model 4000 Spectrophotometer.

Lifetime measurements were made, using the apparatus shown schematically in Figure 9a. Pump light was provided by a 50-joule air spark which has a decay time of 20μ seconds (Figure 9b). The excitation wavelength was selected by passing this light through a Perkin-Elmer Model 12 Monochromator. Fluorescence from the sample was selected by the use of filters or another monochromator. Lifetime was measured by photographing the fluorescence decay curve as displayed on an oscilloscope. The same apparatus was used for excitation and transmission spectra, except that hydrogen and tungsten lamps were used in place of the spark source and readout was accomplished on a Speedomax G as the wavelengths were scanned.

Unless they are indicated as being from other sources, all measurements were made on single crystals grown by the flux technique. The crystals are grown from 99.999 percent pure CeO_2, 99.99 percent pure ThO_2 and reagent $NaBO_2$ flux, unless otherwise noted. The percentage of dopants is based on the percent added to the melt, since distribution coefficients are not known.

2. Transmission Spectra

The transmission spectra of pure and doped CeO_2 and ThO_2 were measured. The primary effort was placed on finding the band edge of CeO_2 and ThO_2, the influence of impurities on the edge, and the possible incorporation of color centers.

a. UV-Visible

Very pure (99.99 percent) CeO_2 was found to be perfectly colorless, having a UV edge at 25,500 cm^{-1} (Figure 10). The addition of 0.1% Ca^{2+} results in an orange-colored crystal with an absorption as shown in Figure 10.

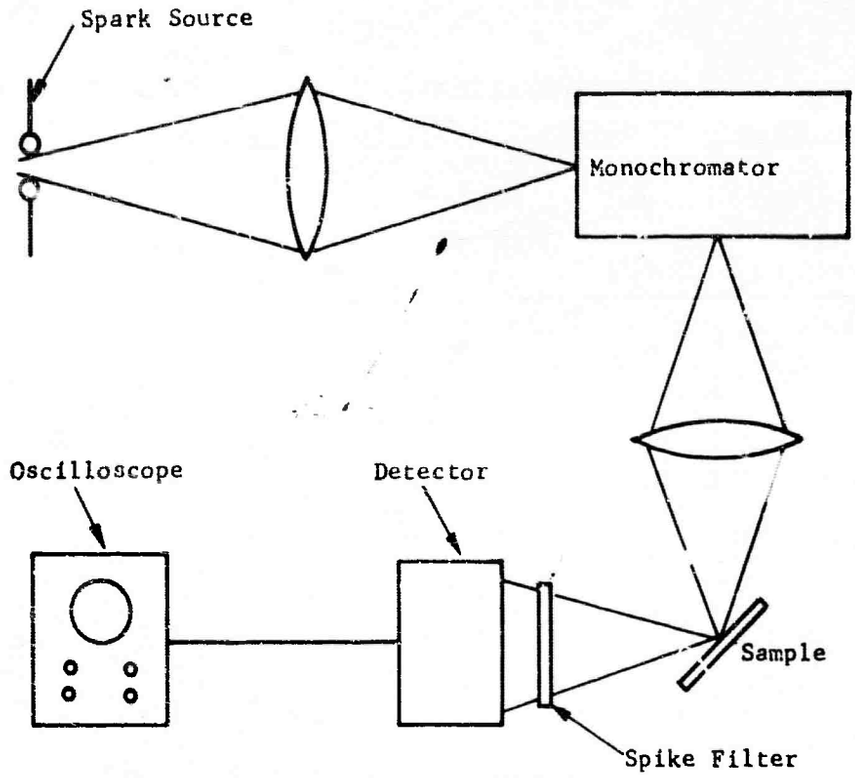

Figure 9a. Fluorescent Lifetime Apparatus

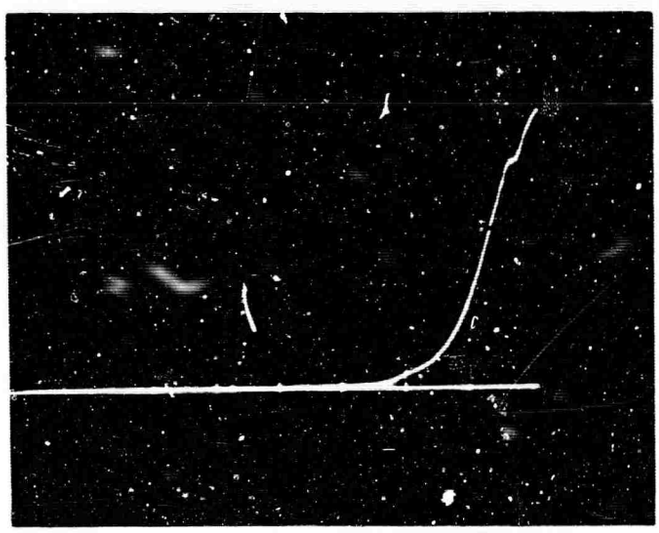

Figure 9b. Oscilloscope Trace of Spark
(Time Scale - 50 μsec/Cm.)

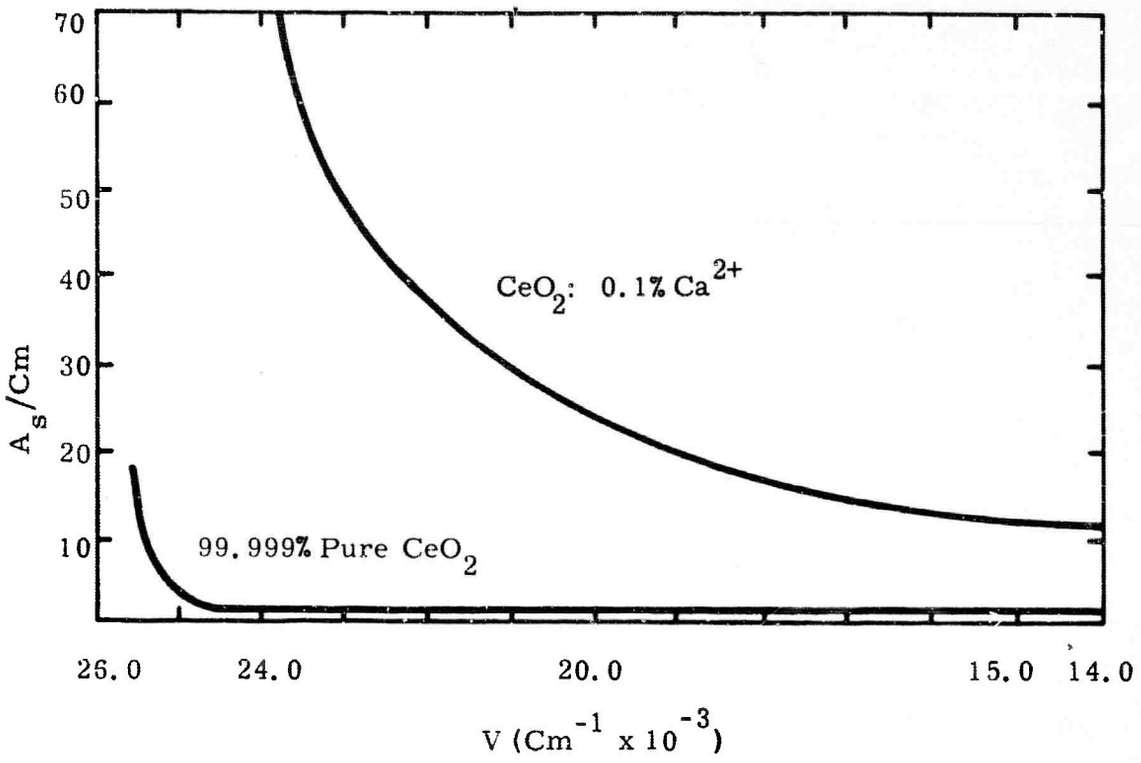

Figure 10. Absorbancy of CeO_2

Since Ca^{2+} does not absorb in these regions, the absorptions are probably color centers caused by the holes necessary for charge compensation. As expected, the colored crystals display higher electrical conductivity than pure CeO_2 if holes are present[6]. Further, the addition of a charge compensating ion such as Mo^{6+} with the Ca^{2+} yields crystals which have no color center. For some reason which is as yet not understood, F^{1-} does not compensate Ca^{2+}. It appears that Pb^{2+} also produces a slightly-colored crystal.

The addition of F^{1-}, Nb^{5+} and Ta^{5+} results in blue crystals. Again, these crystals are characterized by a high electrical conductivity. The blue color can be removed by charge compensating with trivalent rare earths or yttrium.

Thorium oxide has a UV edge near 38,000 cm^{-1}. Figure 11 shows the absorption of 99.9 percent pure ThO_2 and 99.99 percent pure ThO_2 in the UV. It appears that the absorption at 32,000 cm^{-1} is a residual impurity because of its sharp decline in intensity in the purer material. The occurrence of this absorbtion makes accurate determination of the edge difficult.

In the visible region of the spectrum, the same type of color center is seen with Ca additions as with CeO_2, except that the colors are less intense. Fluorine, Y^{3+} and Nb^{5+} gave no color centers. The lack of color centers with F^{1-} additions may be a result of the fact that Th^{4+} is more stable than Ce^{4+}. The Ce^{4+} can be reduced to Ce^{3+}, thereby permitting F^{1-} to substitute for O^{2-}. These color centers are of a permanent nature, and are not bleachable.

A bleachable color center was found in ThO_2 that was grown from lead fluxes. Crystals grown in this manner are perfectly colorless until they are exposed to UV in the 3000Å to 3600Å range, whereupon an absorption develops in the visible. This type of color center is similar to the nonbleachable in its wavelength range; however it bleaches out when the sample is heated to 300°C or stored in the dark for several days. Figure 12 shows the absorption of lead-doped ThO_2 before damage, after a one-minute UV exposure and after a 15-minute UV exposure.

Measurement of the UV transmission showed (Figure 13) that the ThO_2 edge had moved from 2600Å to 3600Å. Analysis of the samples by atomic absorption showed 0.01% lead present. Since Pb^{2+} is known to absorb in this region and damage occurs by pumping this region, it appears that the color center is associated with lead substitution into the ThO_2. Lead substitution

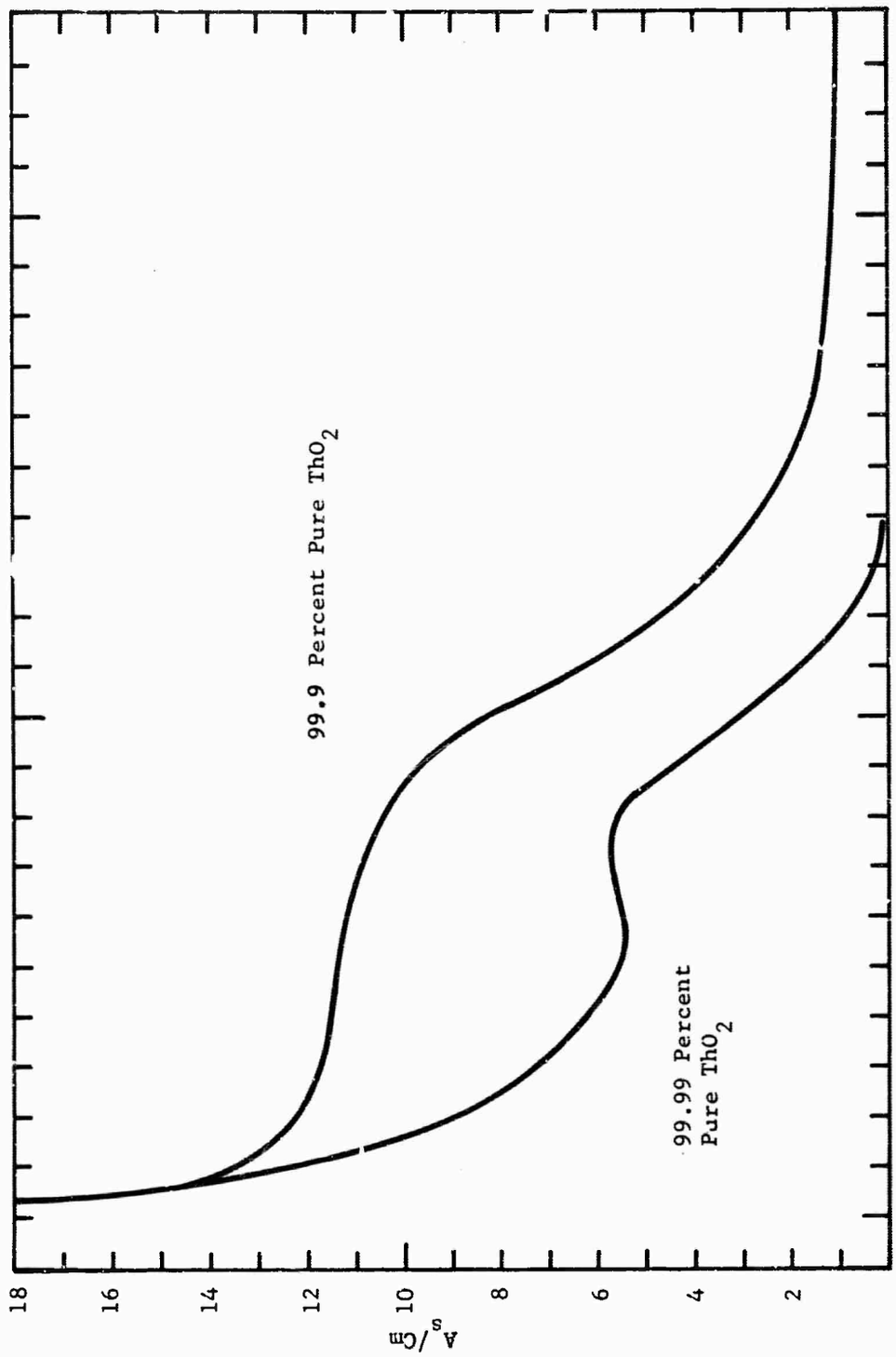

Figure 11. Absorbancy of ThO_2

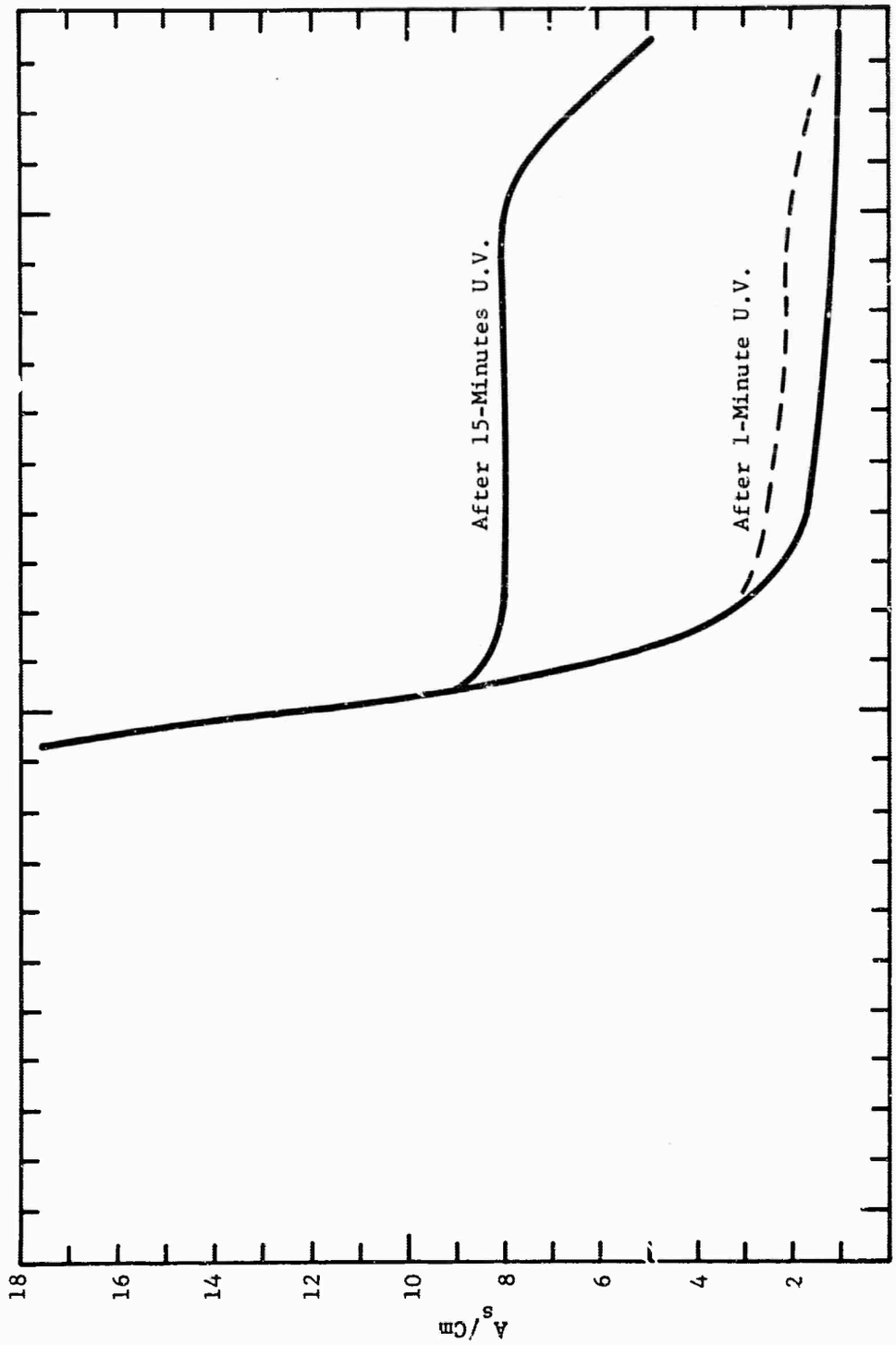

Figure 12. Absorbancy of Lead-Doped ThO_2
(Bleached at 300°C)

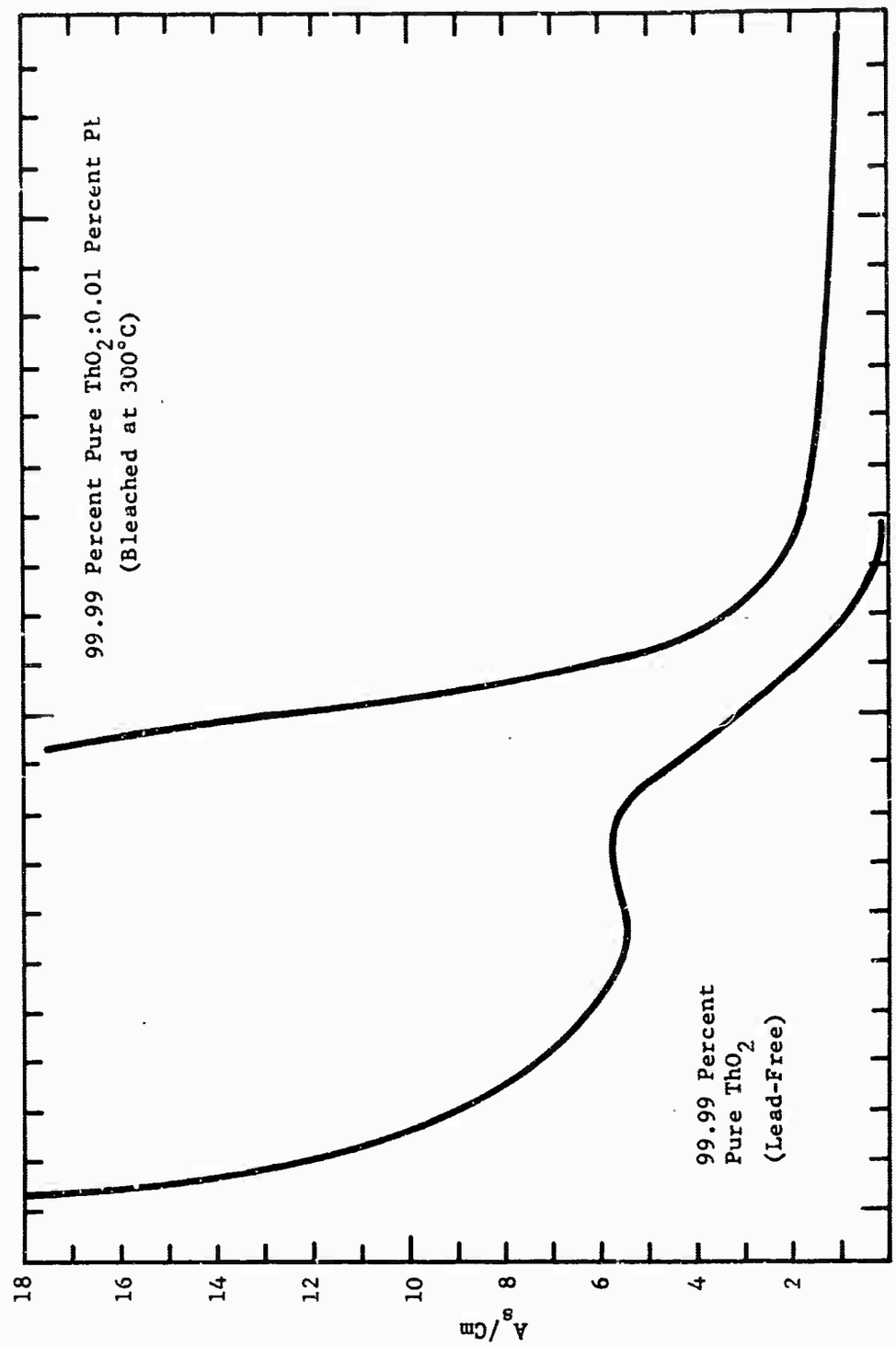

Figure 13. Absorbancy of 99.99 Percent Pure and Lead-Doped ThO_2

into CeO_2 does not cause a bleachable color center because CeO_2 itself is opaque to the light of the damage frequency.

b. Infrared

The infrared spectra to 10μ for CeO_2 and ThO_2 is shown in Figure 14. The infrared cutoff at 8-9μ is better than sapphire, and could make these materials interesting for infrared window applications. The CeO_2 spectra show no extra lines which could be attributed to Ce^{3+} (which has absorptions in the near infrared) indicating that the stoichiometry of the crystals was good.

c. Radiation Damage

Since ThO_2 is radioactive, the possible degrading effect of radiation on its optical properties was studied. The decay of natural thorium (Th^{232}) is as follows:

DECAY REACTION		
$Th^{232} \longrightarrow Ra^{228}$	+ α 3.98 MeV + γ 0.055 MeV	1.39×10^{10} years
$Ra^{228} \longrightarrow Ac^{228}$	+ β 0.030 MeV	6.7 years
$Ac^{228} \longrightarrow Th^{228}$	+ α 4.54 Mev + β 1.5 Mev + γ 0.05-0.96 MeV	6.13 years
Etc. $\longrightarrow Pb^{208}$		

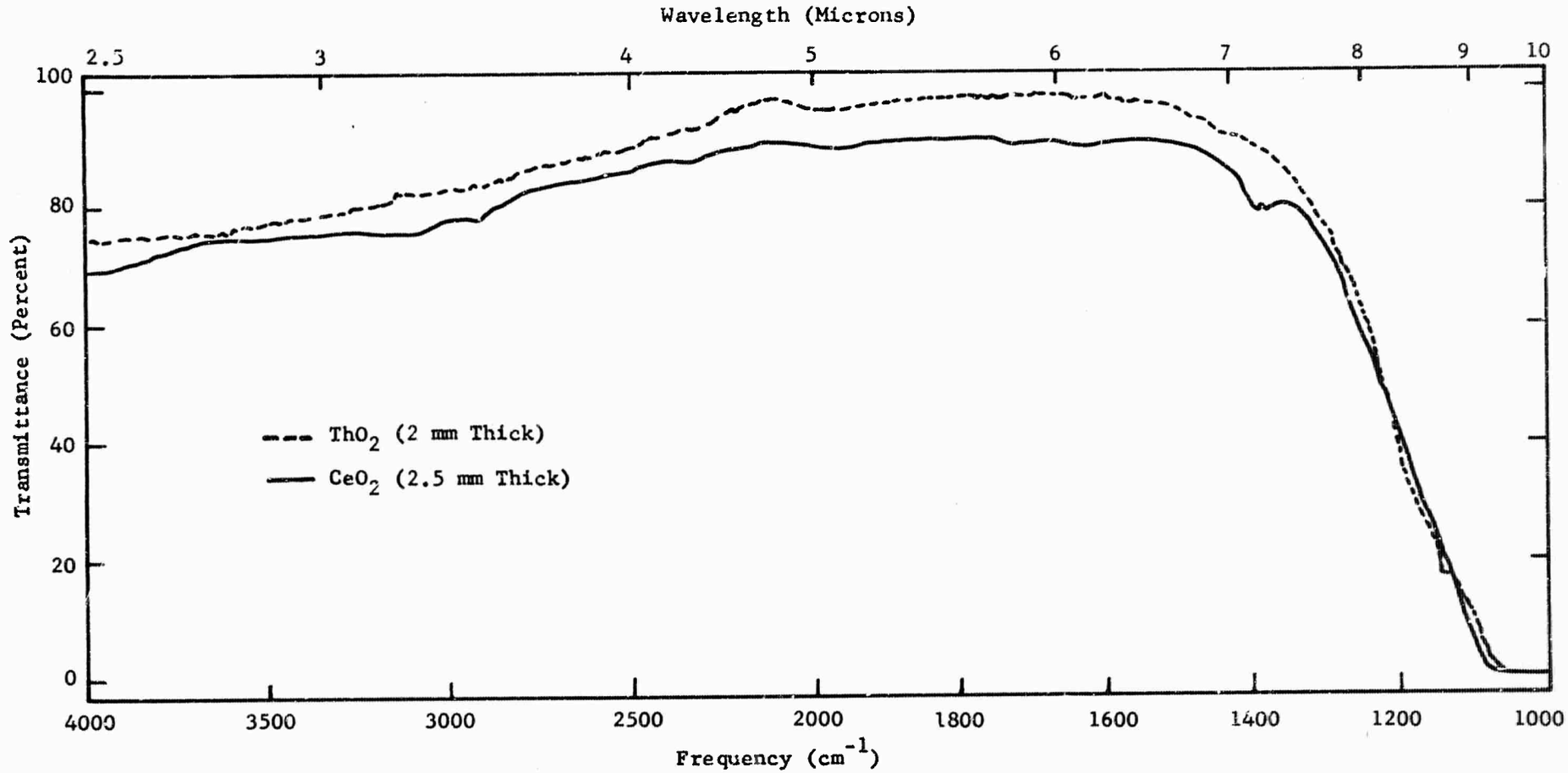

Figure 14. Infrared Cutoff of ThO_2 and CeO_2

For α particles of less than 10 MeV, the coulomb barrier prevents interaction with the nuclei (except for very light elements). Therefore, one would not expect transmutation of the rare earth dopants from the 3.98 MeV α. The α-particles are energetic enough to produce atomic displacements. The possible optical degradation due to the α radiation was not studied directly; however, some indirect experiments were performed. The line emission spectra of residual rare earths in one-year-old ThO_2 reagent was not measurably different from the lines in freshly prepared ThO_2 reagents. There was no detectable thermoluminescence in one-year-old ThO_2, while there is thermoluminescence when it is irradiated with 50 KeV x-rays. This indicates that there is no significant damage to the active ions themselves, or that optical degradation occurred due to long-term 3.98 MeV α radiation.

The low-energy β-radiation is incapable of producing atomic displacements and could only appear as an electron ionization. Optically, β-ionizations could not be differentiated from α-ionizations.

The effects of prolonged 0.055 MeV γ-radiation was simulated by irradiating rare earth doped ThO_2 with 0.05 MeV X-rays. Exposures of 1/2-hour (equivalent to $\sim 10^{10}$ years natural decay) were given to lead-free samples containing Sm^{3+}, Tb^{3+} and Eu^{3+}. After irradiation, all of these samples exhibited a rapidly-decaying phosphorescence at room temperature, and a sharp thermoluminescence (at 85 to 125°C). Samples which were stored after irradiation exhibited sharply decreased (or no) thermoluminescence after three hours to three weeks, depending on the dopant. This indicates that the damage anneals out at room temperature. Transmission measurements on these crystals immediately after irradiation showed no absorptions in the visible region of the spectrum which

could be attributed to trap levels. In addition, the line emission had not changed after irradiation. Thus, it is evident that the 0.055 MeV γ-radiation will not degrade the lead-free ThO_2 optically.

Crystals grown from lead fluxes exhibit extensive color centers from 0.05 MeV x-radiation which are identical to UV damage. Coloration anneals out at room temperature, and would not be expected to accumulate from self-irradiation. A 2-gram, lead-doped ThO_2 crystal stored for a month in the dark showed no detectable color center formation. However, 200 grams of lead-doped ThO_2 crystals stored together in the dark for a month showed appreciable damage because of the high flux density resulting from a large mass of ThO_2.

As a result of the radiation damage experiments described, it is felt that there is no reason to expect degradation of a ThO_2 laser due to its own radioactivity, provided the material is free of lead or other possible color-center inducing ions.

3. Emission

The elements investigated were the trivalent rare earths, divalent manganese, tetravalent niobium and uranium and the noble metal ions. In CeO_2, visible emission was detected only with Sm^{3+}, Eu^{3+} and Er^{3+} doping. It was found that the 99.999 percent pure CeO_2 contained residual Sm^{3+}, which gave its characteristic emission spectra with x-ray excitation. This background of samarium emission was seen in all of the above samples, except those containing Er^{3+} and Dy^{3+}, which are known to quench Sm^{3+}. Therefore, extra lines attributable to Sm^{3+} were seen in the europium-, manganese-, terbium- and uranium-doped samples. Visible emission was seen in ThO_2 with Sm^{3+}, Eu^{3+},

Er^{3+}, Dy^{3+} and Tb^{3+}. There was emission from an unidentified impurity in the 99.99 percent pure ThO_2, which was seen superimposed on the rare earth spectra.

In CeO_2 and ThO_2 infrared emission was observed from Nd^{3+} and Yb^{3+}. The Nd^{3+} emission was a factor of 5 to 10 weaker than a similar sample of $CaWO_4$: Nd and the Yb^{3+} was a factor of 500 weaker than $CaWO_4$: Nd. That no emission was seen from CeO_2 and ThO_2 containing Er^{3+}, Tm^{3+}, Ho^{3+}, Pr^{3+}, Pr^{3+} or U^{4+} is not surprising, in view of the weak emission of Nd^{3+} and Yb^{3+}.

The details of these systems are given below:

a. CeO_2

The emission spectra of Eu^{3+}, Sm^{3+} anf Tb^{3+} were presented in the semiannual report and can be found in Appendix III of this report.

(1) Eu^{3+}

The fluorescent litetime of the Eu^{3+} emission shows a large concentration dependence (Figure 15). The lifetime at 0.05% Eu is 1.7 msec. and falls off to 0.8 msec. at 5% Eu. Eu^{3+} at low concentrations shows marked changes when charge compensation agents are incorporated. Figure 16 shows the effect of adding F^{1-}, Nb^{5+} and Ta^{5+} to crystals that contain 0.05% CeO_2. The maximum lifetime for F^{1-} additions occurs with 0.05% F^{1-}. The maximum lifetime for Nb^{5+} and Ta^{5+} additions occurs at 0.5%. However, it is believed that this may only reflect a poor distribution coefficient for Nb^{5+} and Ta^{5+}. The maximum lifetime of any sample was 3.0 msec. with 0.05% Eu^{3+} and 0.5% Ta^{5+}. A variation of charge compensation in the 0.5 or 5.0% Eu sample has no effect on the lifetime.

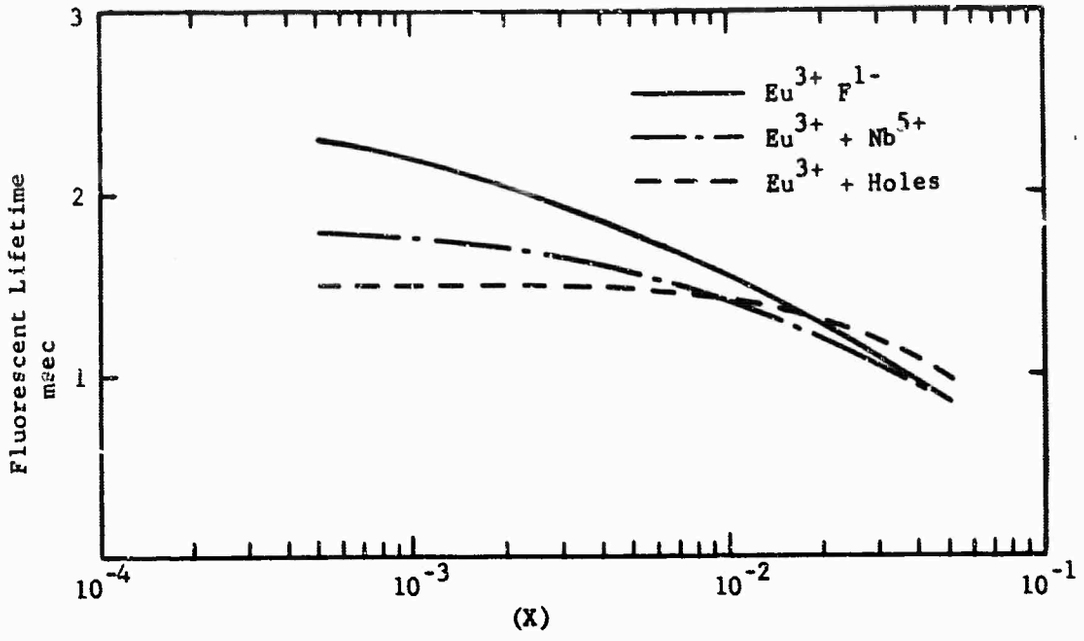

Figure 15. Fluorescent Lifetime of Eu^{3+} in $Ce_{1-x}Eu_xO_2$

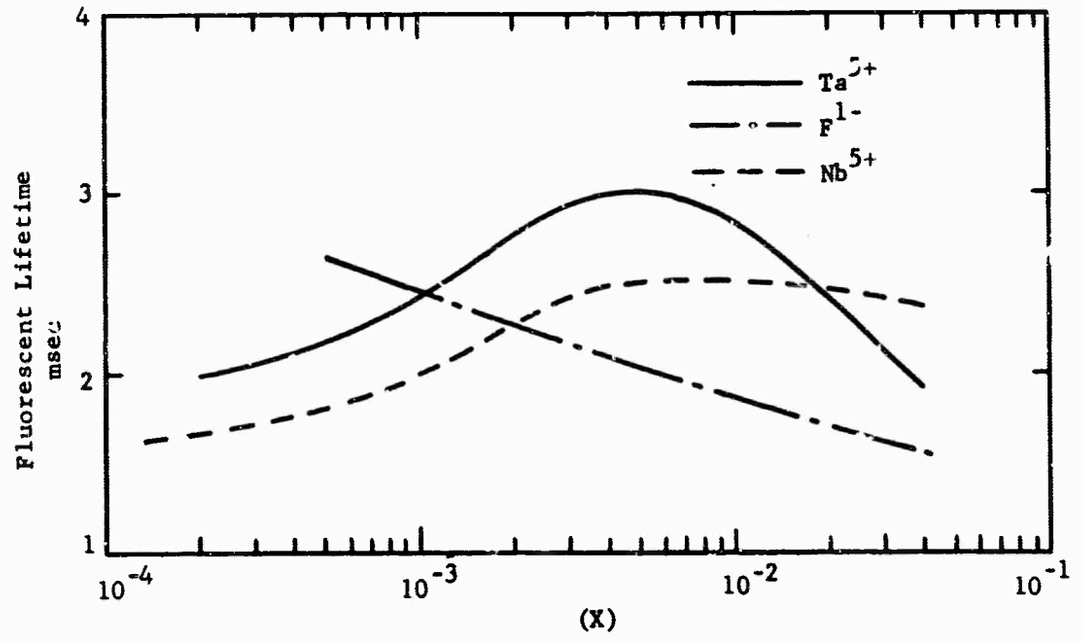

Figure 16. Fluorescent Lifetime of 0.05% Eu^{3+} in $Ce_{1-x}(Nb,Ta,F)_xO_2$

In view of measurements made on Er^{3+} and Yb^{3+} in ThO_2 that were previously cited, it is believed that the decrease in lifetime with concentration can be attributed to a change in site symmetry from mostly cubic to mostly trigonal or a mixture of sites. Incorporation of F^{1-} or Nb^{5+} into dilute samples possibly increases the lifetime by annihilation of the holes, resulting in charge neutrality and increasing the symmetry slightly. The addition of compensation in higher concentration than the europium content places the charge compensation closer to Eu^{3+}, thus distorting the cubic site. Finally, fluorine or niobium compensation has no effect on the more concentrated samples, because fluorine or niobium will always be a near neighbor to some Eu ion, thereby distorting its symmetry.

Similar effects were observed with other rare earths in CeO_2 and ThO_2. Despite the increases in fluorescent lifetime, it should be pointed out that these are not dramatic increases, as in the case of Cr^{3+} in $LaAlO_3$,[7] and are probably not important from the device standpoint.

Transmission spectra of 5% Eu in CeO_2 show the usual absorptions attributable to Eu^{3+}; however these are extremely weak. The excitation spectra (Figure 17) of the 5910Å Eu^{3+} line shows excitation only from 3880Å to 3940Å. This level is in the CeO_2 absorption edge and its efficiency is probably due to energy transfer from the CeO_2. Since this major excitation band does lie in the CeO_2 edge, it will not be possible to optically pump thick crystals.

(2) $\underline{Nd^{3+}}$

The room temperature emission spectra from 10,500 to 10,900Å of 1% Nd^{3+} is shown in Figure 18. The strongest line of the 10,600Å group is found at

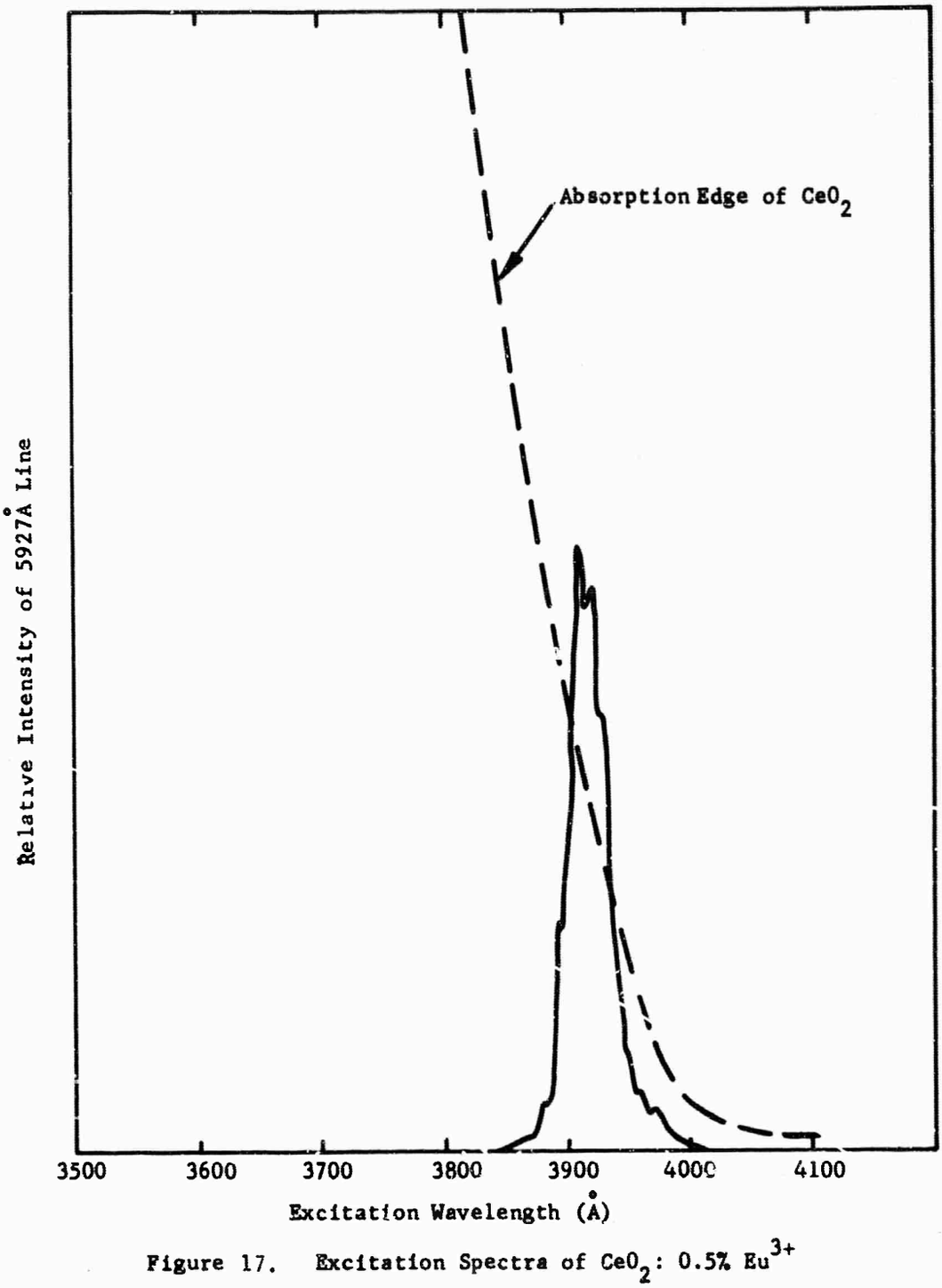

Figure 17. Excitation Spectra of CeO_2: 0.5% Eu^{3+}

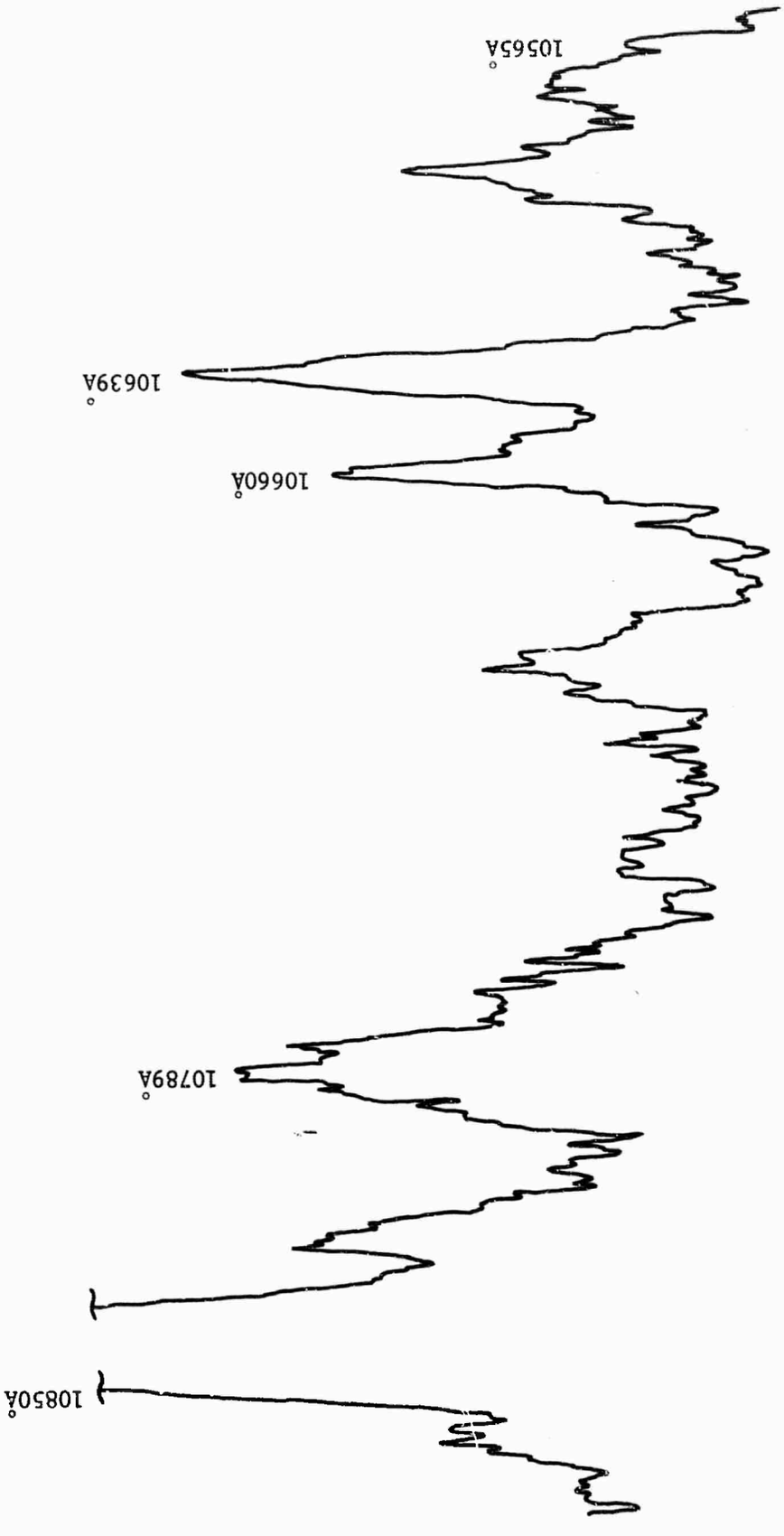

Figure 18. Emission Spectra of $CeO_2:Nd^{3+}$ (Room Temperature)

10,639Å and is 11Å wide. Unlike $CaWO_4$: Nd, the line at 10,857Å, which is 13Å wide, is much stronger than the 10,600Å lines. The fluorescent lifetime of the 1% sample is 340μ seconds.

The excitation spectra showed no new excitation bands. Experiments intended to study energy transfer showed no energy transfer to Nd^{3+} from U^{4+}, Mn^{2+}, Te^{4+}, or Nb, Tb, and Pr, which were of mixed valence.

(2) Yb^{3+}

The emission of Yb^{3+} in CeO_2 is so weak at room temperature that it is barely detectable. Cooling to liquid nitrogen increases the brightness by a factor of 50. However, it is still so weak that broad slits are needed in order to observe it, so that it is impossible to resolve all the lines. The spectra obtained (Figure 19) shows two lines at 10,402 and 10,288Å. These were found to be about 20 and 25Å wide, respectively; however, this may still be instrument-broadened.

b. ThO_2

(1) Eu^{3+}

The emission spectra of Eu^{3+} in ThO_2 is similar to Eu^{3+} in CeO_2. The strong lines are listed in Table II. Of particular interest is the line at 5903Å which is 3.5Å wide at room temperature and 1Å wide at liquid nitrogen. These are of the same width and lifetime as in CeO_2. However, they are a factor of 100 brighter than in CeO_2. This occurs because the UV edge of ThO_2 is at a shorter wavelength, thereby allowing the pump light to utilize most of the Eu^{3+} absorptions.

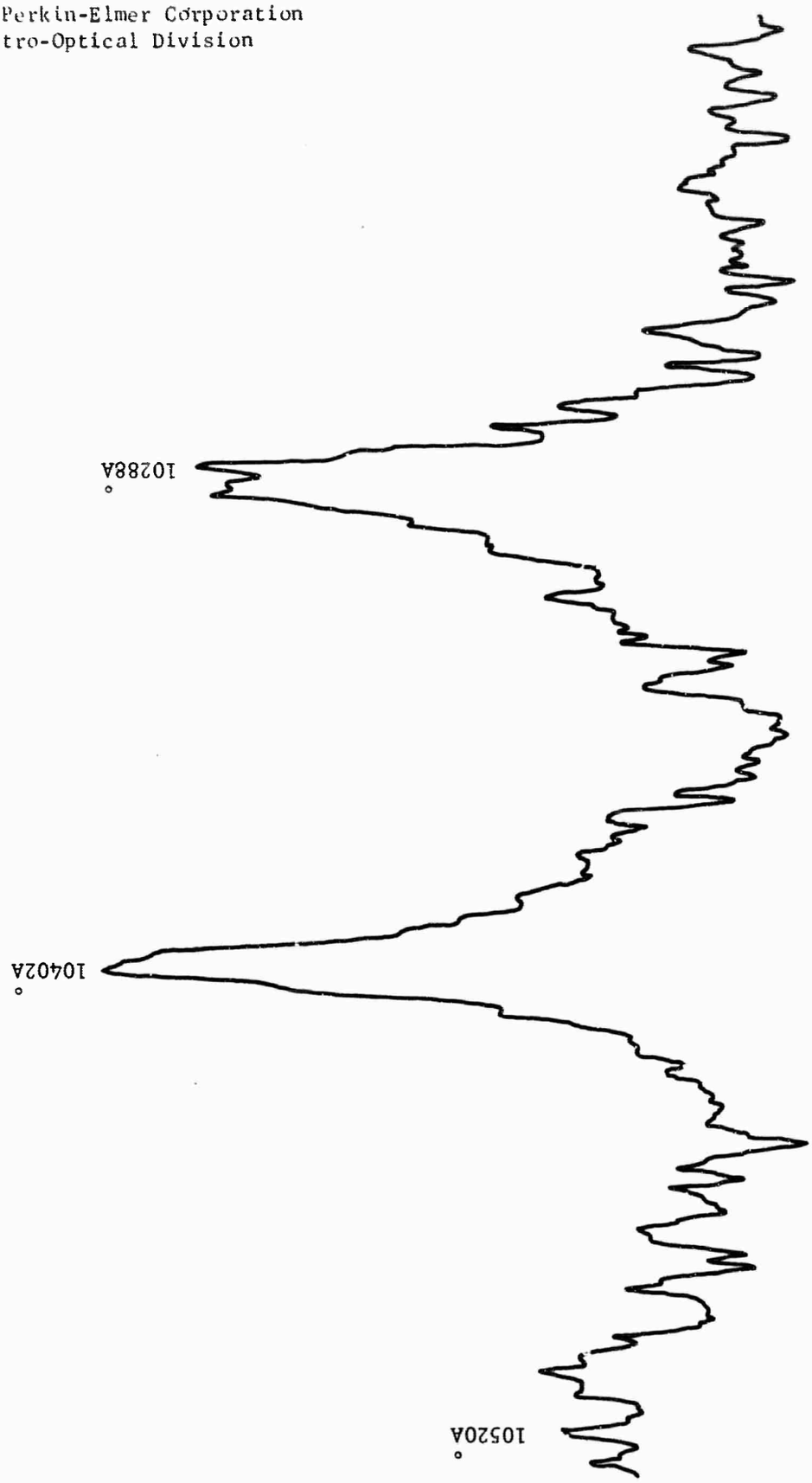

Figure 19. Emission Spectra of $CeO_2 : Yb^{3+}$ (77°K)

TABLE II

ROOM TEMPERATURE EMISSION OF ThO_2 : 0.05% Eu

λÅ	ΔλÅ	Relative Intensity (Corrected for Photo-multiplier Response)
5845		0.27
5873		0.47
5877		0.37
5903	2.5	0.91
5923		0.16
5945		0.29
6067		0.13
6108	16	0.60
6300	9	1.00

In order to investigate the effect of concentration and charge compensation on the spectra, the ^5D_o to $^7F_1$ transition was studied. It was found necessary to make these measurements at liquid nitrogen, to observe the small separations. The spectra of ThO_2 containing 0.5% Eu^{3+}, 0.5% Eu^{3+} plus F^{-1}, and 0.5% Eu^{3+} plus 0.5% Ta^{5+} are shown in Figure 20.

The gross effects are that F^{-1} compensation practically eliminates the 5858, 5844, 5967, 5872 and 5874Å lines and introduces 5895, 5898 and 5909Å lines. Ta^{5+} eliminates the same lines as F^{-1}, but has the effect of broadening the remaining lines. The 5902Å line, for instance, is broadened from 1Å to 3.7Å. In experiments where only minute amounts of F^{-1} were added to the melt, the same lines disappeared, but the 5895, 5898 and 5909Å lines were not enhanced. In samples of low concentrations, the 5895, 5898 and 5909Å lines are strong; in fact, these decrease in intensity with increased Eu^{3+} concentration. The 5884 and the 5902Å lines remain substantially unchanged in relative intensity with concentration and charge compensation. It appears from this data that there may be up to four spectra present, probably representing four sites.

Attempts were made to measure the fluorescent lifetime of the individual lines. However, the lines were not of sufficient brightness to permit convenient measurement of individual lifetimes.

(2) Sm^{3+}, Er^{3+}, and Dy^{3+}

The spectra of Sm^{3+}, Er^{3+} and Dy^{3+} in ThO_2 are not substantially different from the same ions of CeO_2 or other hosts. Since these lines were found to be very broad, they were not studied in detail.

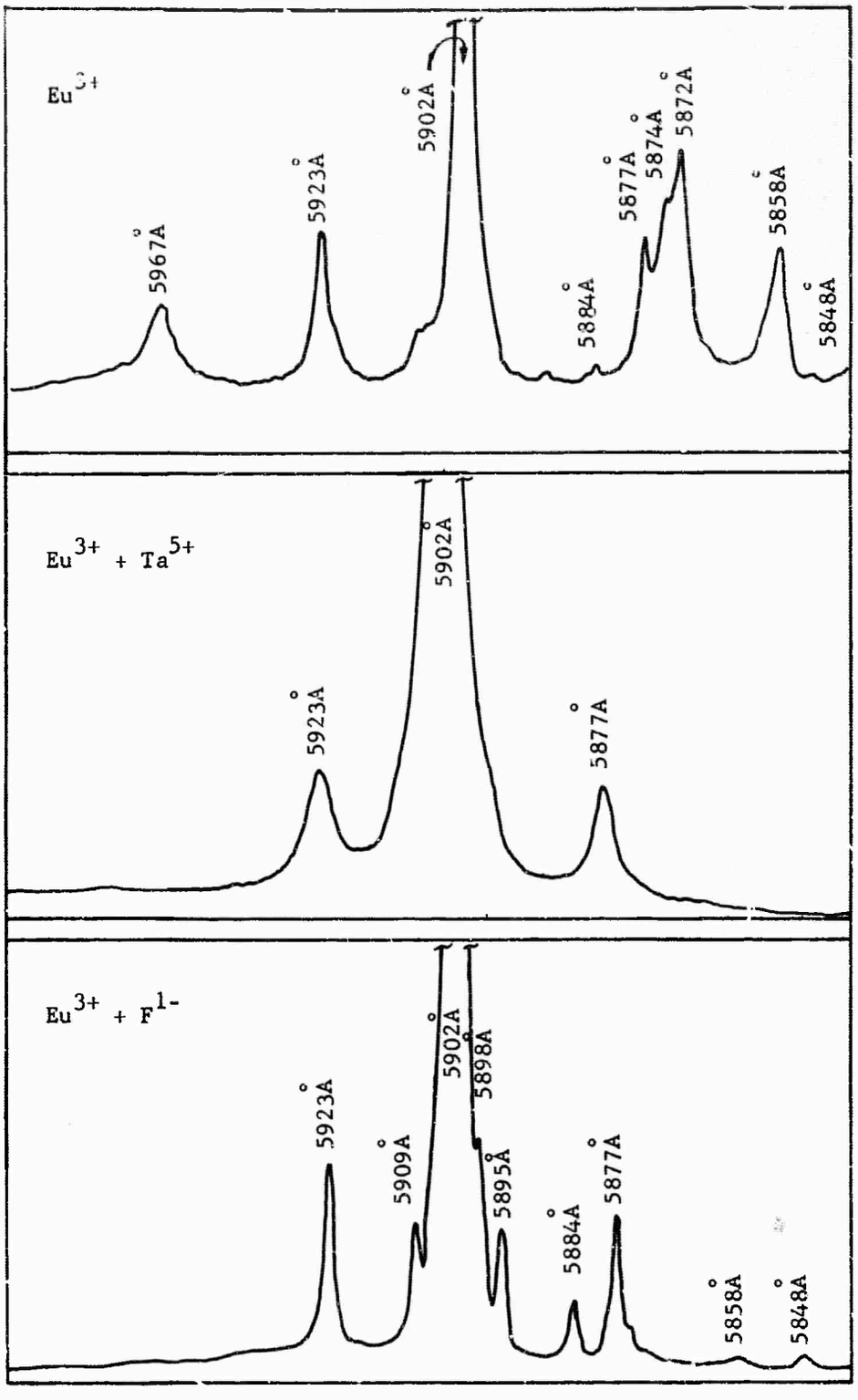

Figure 20. Emission of Eu^{3+}, ^5D_o - $^7F_1$ Transition in ThO_2 at 77°K

(3) $\underline{Tb^{3+}}$

In ThO_2, Tb^{3+} fluoresces brightly. Emission spectra of the strong lines are illustrated in Figure 21. The strongest line, at 5433Å, is 5.4Å wide. In ThO_2 doped with terbium, there is no coloration of the crystals as in CeO_2. This is probably due to the more stable nature of Th^{4+}. Energy transfer from Tb^{3+} to Eu^{3+} was observed in ThO_2.

(4) $\underline{Nd^{3+}}$

The emission spectra of the strong lines of Nd^{3+} in ThO_2 grown from PbF_2 flux are shown in Figure 22. The strongest line occurs at 10608Å, and is 11Å wide. At liquid nitrogen, this narrows to 3.5Å. As in the case of CeO_2, Nd^{3+} in ThO_2 is considerably weaker than in $CaWO_4$. The fluorescent lifetime of Nd was found to be 400μ seconds.

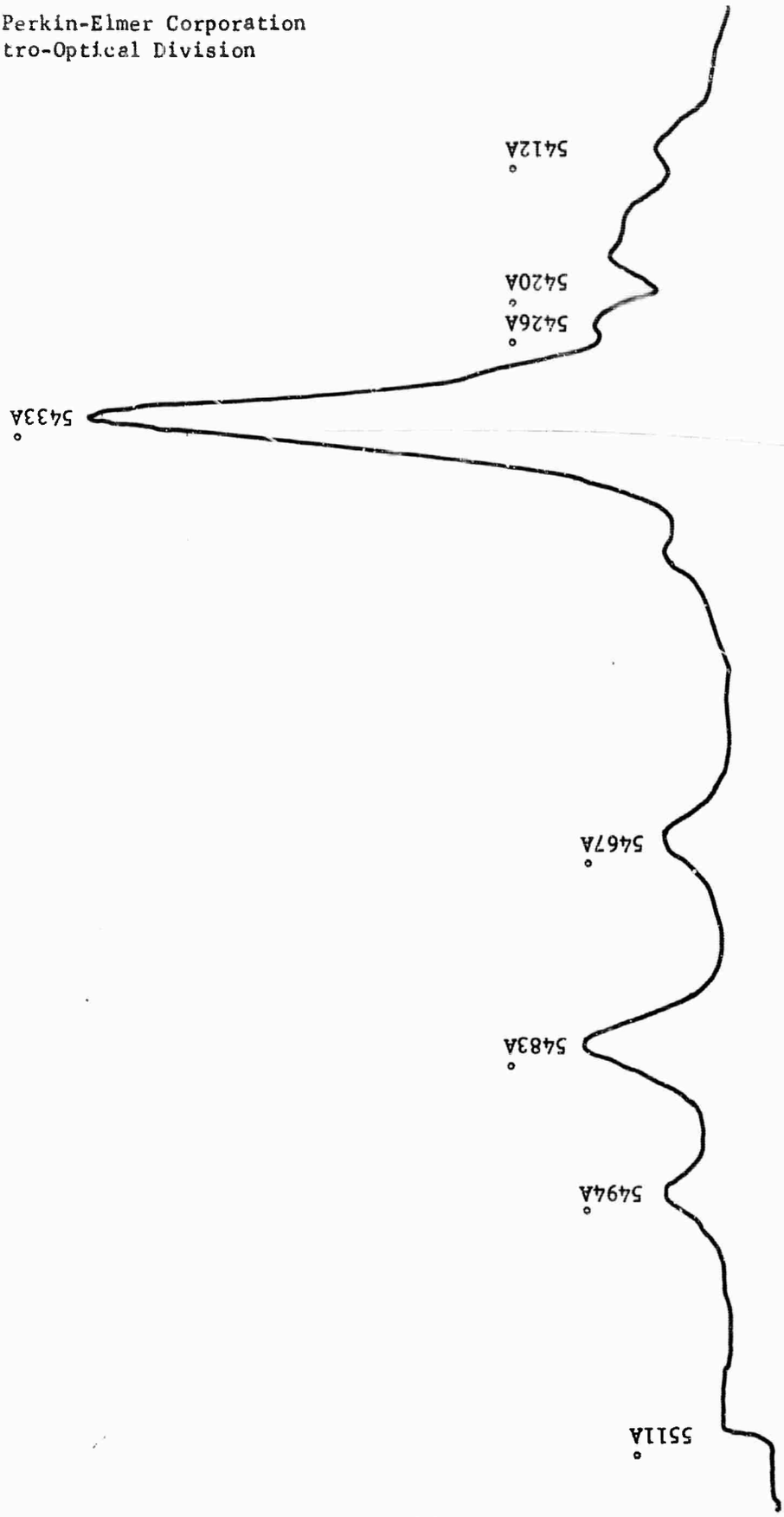

Figure 21. Emission Spectra of $ThO_2:Tb^{3+}$ (Room Temperature)

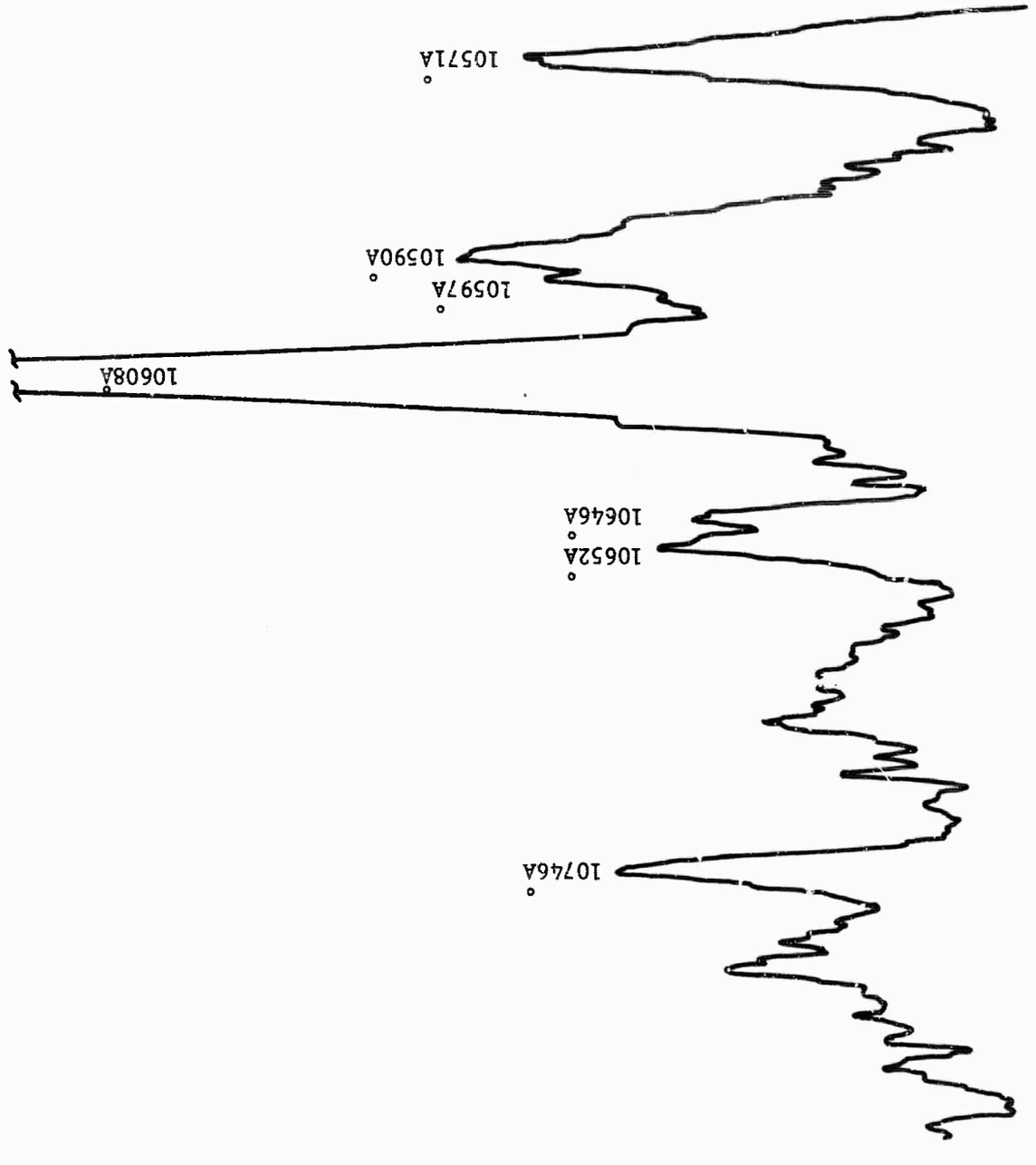

Figure 22. Emission Spectra of $ThO_2:Nd^{3+}$ (Room Temperature)

SECTION IV

LASER TESTING

Tests for laser action were made on neodymium-doped CeO_2 and ThO_2. The CeO_2 rod (grown from $Li_2Mo_2O_7$ flux) was 2 mm long by 1 mm diameter. The ThO_2 rod (grown from PbF_2-NaF-B_2O_3 flux) was 11 mm long by 3 mm diameter. Both rods had ends coated to give 99 percent reflection at 1.06μ.

The CeO_2 rod developed a crack during fabrication which enlarged during optical pumping, resulting in a broken rod. Time did not permit fabrication of a new rod.

The ThO_2 rod was tested, using a saturated $NaNO_2$ solution as a filter (UV cutoff 4000Å) to prevent UV damage to the crystal. It was observed that damage did occur with 300 J input to the xenon flash lamp, indicating that a small portion of the light is transmitted by the filter. The damaged crystal did not lase. It is believed that no lasing occurred for two reasons: first, color center absorption lies at the same wavelength as the neodymium absorptions; and second, it is possible that a two-photon loss process is occurring as observed with Er^{3+} in CaF_2.[8] High intensity flash exposures on neodymium-doped crystals grown from lead-free fluxes showed no damage, indicating that no color centers form from rare earth doping, and that a laser probably can be made when large, lead-free crystals are obtained.

SECTION V

CONCLUSIONS

We have learned to grow pure and doped CeO_2 and ThO_2 by the flux technique. Crystals of ThO_2 suitable for laser testing have been grown. Measurements on these crystals indicate that ThO_2 is preferable because of many superior properties, such as: better crystal quality, transmission range, little color center formation, and greater fluorescent brightness. However, the initial goal of achieving extremely long lifetimes was not attained. This raises doubt of the merit of high-symmetry hosts for trivalent rare earths, especially when charge compensation is required which results in an increase in the number of emission lines observed.

BIBLIOGRAPHY

[1] M. Abraham, R.A. Weeks, G.W. Clark and C.B. Finch, Phys. Rev. 137, A138 (1965).

[2a] J. Makovsky, Presented Third Conference on Quantum Electronics (1965).

[b] G.D. Boyd, R.J. Collins, S.P.S. Porto and W.A. Hargreaves, Phys. Rev. Letters, 8, 269 (1962).

[3a] A.B. Chase and J. Osmer, Am. Min., 49, 1469 (1964).

[b] C.B. Finch and G.W. Clark, J. Appl. Phys. 36, 2143 (1965).

[4] R.A. Laudise, R.C. Linares, E.F. Dearborn, J. Appl. Phys. Suppl. 33, 1362 (1962).

[5] J. Makovsky, W. Low and S. Yatsiu, Phys. Letters, 2, 187 (1962).

[6] C.J. Kevane, E.L. Holverson and R.O. Watson, J. Appl. Phys. 34, 2083 (1963).

[7] R.C. Ohlman, Bulletin Am. Phys. Soc. 9, 281 (1964)

[8] M.R. Brown, and W.A. Shand, Phys. Letters, 18, 95 (1965)

APPENDIX I

PHASE EQUILIBRIA AND SOLUBILITIES IN CeO_2-FLUX SYSTEMS

APPENDIX I

PHASE EQUILIBRIA AND SOLUBILITIES IN CeO_2-FLUX SYSTEMS

1. Phase Equilibria

Phase equilibria and solubilities of CeO_2 in various flux systems are detailed in this Appendix. The phase equilibria were determined as described in the text.

a. PbO-PbF_2-B_2O_3

CeO_2 was found to be the stable solid phase in the PbO-PbF_2-B_2O_3 in any combination of the three which contained less than 25 mole percent B_2O_3 (Figure 1). When more than 25 percent B_2O_3 is used, $CeBO_3$ often co-precipitates with CeO_2 at lower temperatures; with more than 75 percent B_2O_3, a miscibility gap formed.

b. Na_2O-B_2O_3-MoO_3

The stability points for CeO_2 in the system Na_2O-B_2-O_3-MoO_3 are shown in Figure 2. Here again there is a liquid miscibility gap with a high B_2O_3 content; however, the stability region of CeO_2 is much more limited than in the lead system. On the Na_2O-MoO_3 edge there was only one composition that yielded any CeO_2. Even this was mixed with $NaCeMo_2O_8$, which forms in all other cases. When B_2O_3 is substituted for MoO_3 in these compositions the CeO_2 is again formed.

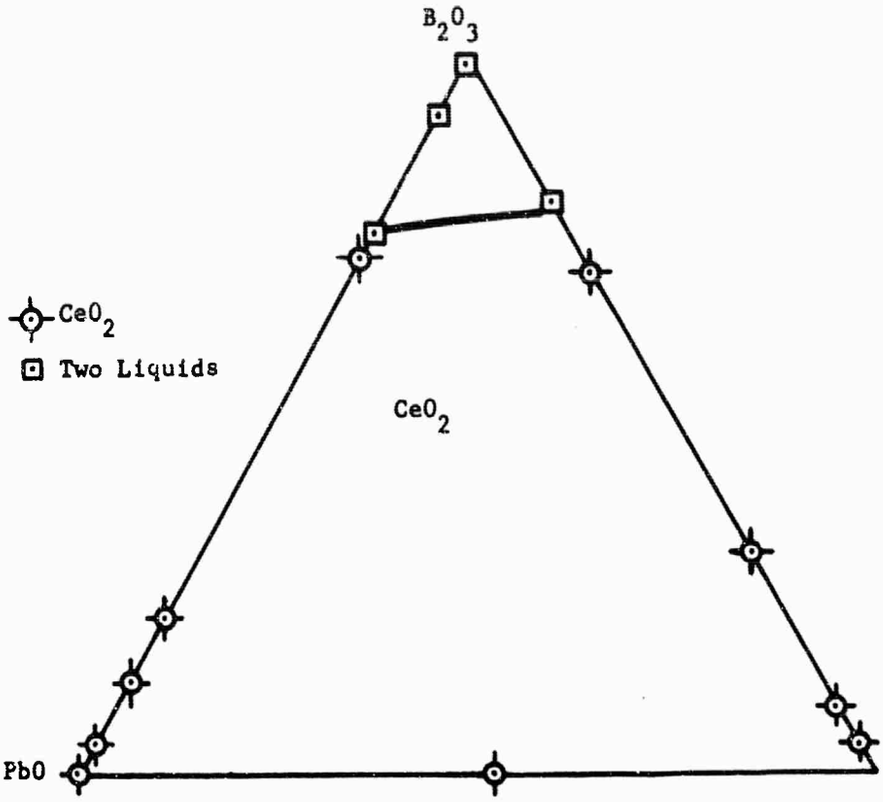

Figure 1. System CeO_2 - (B_2O_3 - PbO - PbF_2) from 1300° C to 950° C

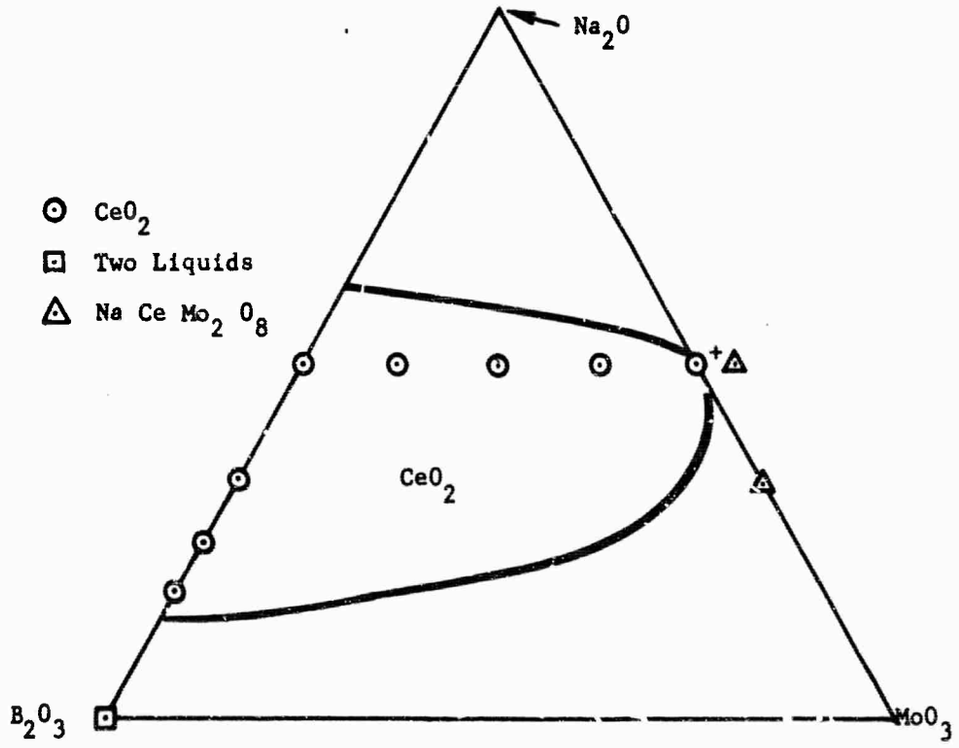

Figure 2. System CeO_2-(Na_2O - B_2O_3 - MoO_3) from 1300°C to 950° C

c. Li_2O-B_2O_3-MoO_3

CeO_2 is stable in the Li_2O-B_2O_3-MoO_3 systems using most ratios of MoO_3/B_2O_3, provided Li_2O is present between 10 and 60 mole percent (Figure 3). $LiCeMo_2O_8$ was found to form in the molybdate melts at temperatures below 800°C.

2. Solubilities

a. CeO_2

The solubilities of CeO_2 in some of the flux compositions were determined by the quench melt technique. These compositions were selected because of their potential for growing large crystals of CeO_2. The solubility points were made by holding the melt in contact with undissolved CeO_2 at the desired temperatures for 24 hours. At the end of this time, the liquid containing dissolved CeO_2 was decanted and frozen. It was then analyzed for CeO_2 content by wet chemical methods.

The solubility curve for CeO_2 in $NaBO_2$ is shown in Figure 4. Here the solubility varies from 7 percent at 1300°C to 1.7 percent at 950°C. While this does not have a high solubility for CeO_2, almost all of the CeO_2 can be recovered upon cooling, thereby allowing reasonable yields of crystals.

The solubility of CeO_2 in $Li(Mo_xB_{1-x})_4O_y$ is shown in Figure 5 as a function of x. The highest solubility is found in the high boron fluxes. A plot of the slope of solubility versus temperature shows the slope to be proportional to the boron content of the flux (Figure 6). Figure 7 shows the solubility of CeO_2 in $Li(Mo_xB_{1-x})_2O_z$. Here the slopes change as above, but the solubilities are slightly lower. Thus, it is possible by slight flux modifications to vary slope and solubility in a particular crystal-growing experiment.

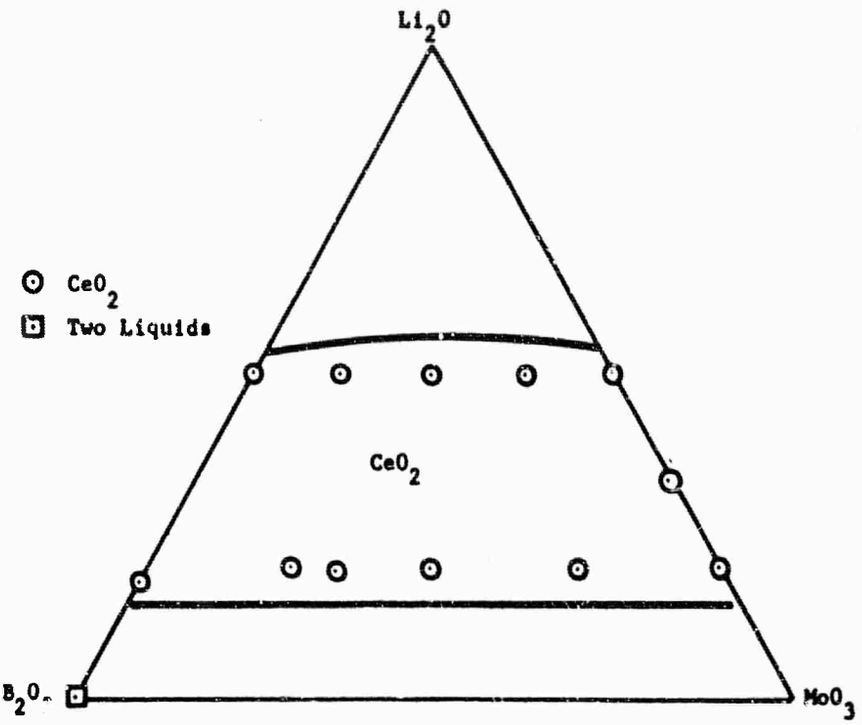

Figure 3. System CeO_2 - (Li_2O - B_2O_3 - MoO_3) from 1300°C to 950°C

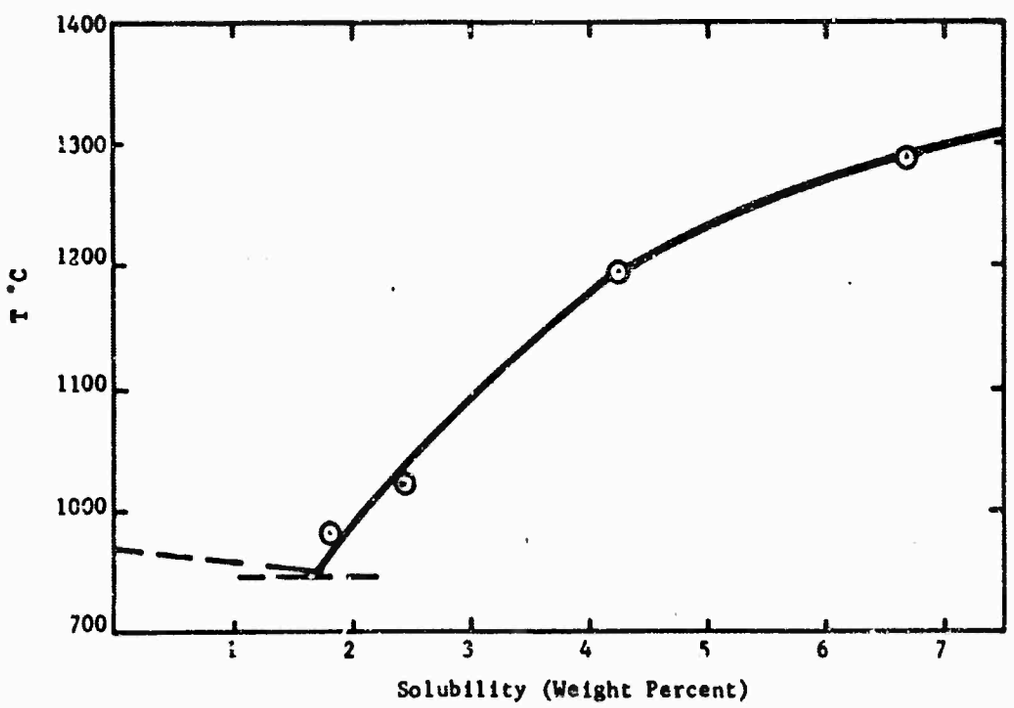

Figure 4. Solubility of CeO_2 in $NaBO_2$

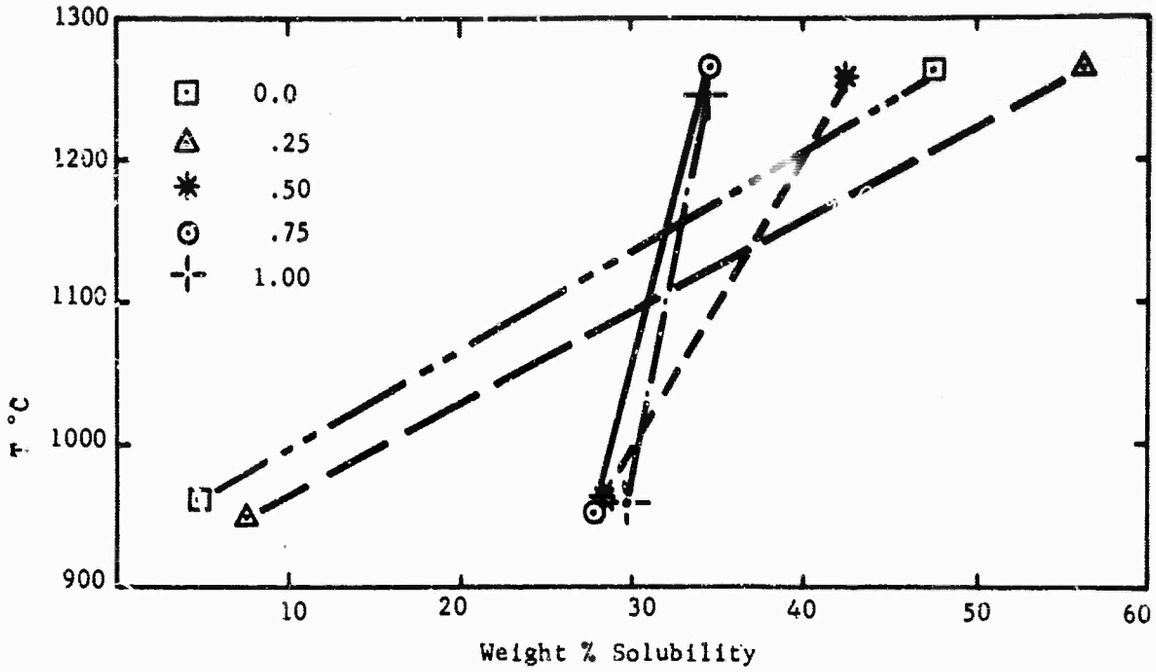

Figure 5. Solubility of CeO_2 (Wt. %) in Li $(Mo_x B_{1-x})_4 O_y$

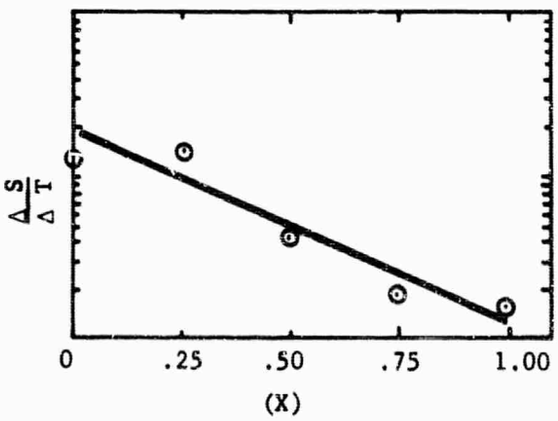

Figure 6. Slope of Solubility of CeO_2 $(\frac{\Delta S}{\Delta T})$ in $Li(Mo_x B_{1-x})_4 O_y$

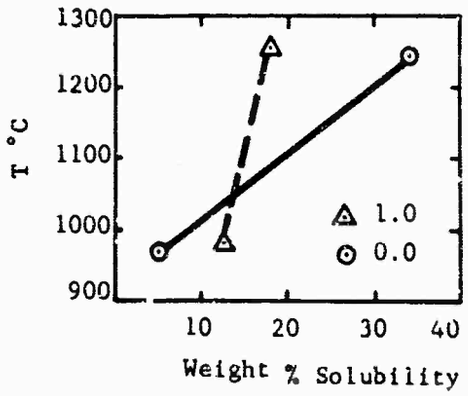

Figure 7. Solubility of CeO_2 (Wt. %) in Li $(Mo_x B_{1-x})_2 O_z$

The solubility in lead flux system was not determined. However, it increases significantly with higher PbF_2 content.

APPENDIX II

THE APPLICATIONS OF X-RAY-EXCITED OPTICAL FLUORESCENCE TO ANALYTICAL CHEMISTRY

The Perkin-Elmer Corporation
Electro-Optical Division

Report No. 8197

APPENDIX II

THE APPLICATIONS OF X-RAY-EXCITED OPTICAL FLUORESCENCE TO ANALYTICAL CHEMISTRY

R.C. Linares, J.B. Schroeder and L.A. Hurlbut

The Perkin-Elmer Corporation
Norwalk, Connecticut 06852

ABSTRACT

Apparatus for measuring the x-ray excited optical emission spectra is described. A technique is described for quantitatively measuring the concentration of Tb, Dy, Eu and Gd in Y_2O_3. The limits of detectivity were found to be 0.02, 0.03, 1.0 and 1.0 ppm respectively. A method for substantially reducing these limits is given. The limit of detectivity for rare earth impurities in synthetic garnets and CeO_2 appears to be comparable to that measured in Y_2O_3.

Presented at the Pittsburgh Conference on Analytical Chemistry, March 1-6, 1955.

Published in Spectrochimica Acta, 21, 1915 (1965).

During the investigation of the optical properties of rare-earth-doped synthetic garnets, it was noted that the x-ray excited optical emission spectra was very sensitive to rare earth contamination. In fact, a sample of chromium-doped gadolinium gallium garnet ($Gd_3Ga_5O_{12}$:Cr) in which only the chromium fluorescence could be detected with ultraviolet excitation showed emission lines attributable to many of the rare earths when excited with 50 KeV x-rays. This pronounced sensitivity to rare earth impurities prompted us to examine the possibility of adapting the technique for routine quantitative analysis of incoming rare earth oxides. Because of other programs in our laboratory, high purity Y_2O_3 was selected for the initial investigation.

METHOD

Early work[1] indicated that x-rays were not suitable for the excitation of optical spectra. This result appears to have been caused by an unfortunate choice of samples and the use of high energy x-rays. More recently, Low demonstrated that x-rays were a very suitable means for exciting the rare earth fluorescence.[2] Low[3,4,5] also has demonstrated the usefulness of x-rays in exciting chromium, nitrogen, semiconductors, etc. In other words, it is a completely general technique for gases and solids. Liquid samples, on the other hand, have not yielded satisfactory results to date.

The details of the excitation mechanism are not known. However, it seems likely that x-rays excite photoelectrons in the host lattice as well as the characteristic x-ray fluorescent spectra. The photoelectrons then preferentially transfer their energy to impurity atoms by inelastic scattering. Direct absorption of x-rays by the impurity atom is certainly not the

primary method of excitation. One tenth percent rare earth in Y_2O_3 would absorb approximately 0.0005 times as much of the incident x-ray energy as the yttrium and this certainly is not adequate to account for the bright visible fluorescence observed.

X-ray excitation has the very important advantage over ultraviolet excitation that the spectral match between the ion under investigation and the source is no longer important. This enables one to effectively excite ions with narrow or weak absorption bands. Further, the energetic photoelectrons excite the impurities to a higher state than does ultraviolet excitation. Therefore, all of the allowed optical transitions can be observed, not just those originating at levels below the energy of the pump. Another fundamental advantage of x-ray excitation is that there is no interference between the source and the optical spectra because x-rays are not reflected and, therefore, can be easily kept away from the detector.

EXPERIMENTAL PROCEDURE

The experimental apparatus is shown schematically in Figure 1. X-rays impinge on the sample while it is being viewed with a suitable monochromator. Because of x-ray absorption in the sample and optical scatter (polycrystalline samples only) and absorption, it is advisable to view the front of the sample as indicated. This geometry also reduces the coloration of the optical elements.

During irradiation, the sample was approximated 6 cm from the focal spot of a Machlett OEG-50 tube (Machlett Laboratories, Springdale, Connecticut). The tube was operated at 50 KeV and 40 ma dc. The optical fluorescence was

chopped at 13 cps before entering the slits of a Perkin-Elmer Model 210 monochromator with a 640 lines/mm grating (Figure 2). The slits were sufficiently closed to allow resolution of the line spectra being observed. The signal was detected with a 6705 photomultiplier (S-10 surface) and the signal amplified with a lock-in amplifier (Princeton Applied Research Model JB-5) and recorded with a Leeds and Northrup Speedomax G.

The materials used were Y_2O_3 containing less than 1 ppm total rare earth impurities and rare earth oxides containing less than 10 ppm total rare earth impurities according to the suppliers' assay (Michigan Chemical Company and American Potash & Chemical Company). The samples were prepared by dissolving the desired amount of Y_2O_3 and rare earth oxide in hot 25 percent HNO_3. The low doping level samples were prepared by successive dilutions of the more concentrated standards. The solution was boiled to dryness and fired at 750°C to yield the doped oxide. The powdered sample was then pressed into an aluminum cup which is attached to the cold finger of the dewar (Figure 3). In addition to providing cooling when desired, the dewar effectively absorbs the x-rays scattered by the sample.

RESULTS

The absorption and emission spectra of most rare earths in Y_2O_3 (using UV excitation) has been reported.[6,7,8,9] The optical emissions occur at the same energies as reported in the literature in the Y_2O_3 and yttrium aluminum garnet, ($Y_3Al_5O_{12}$, except that more weak lines can be seen. However, in the case of Pr^{3+}, visible emission is seen only in the garnet at room temperature. At 77°K a weak, broad band does appear in Y_2O_3:Pr samples. For this

reason no additional measurements were made on Y_2O_3:Pr. Figure 2 shows the emission spectra of 1 atomic percent Eu^{3+}, Gd^{3+}, Tb^{3+} and Dy^{3+} in Y_2O_3 at room temperature. The positions of the lines are conveniently located in that the strong lines of different rare earths do not overlap.

To investigate the sensitivity of this technique, various dilutions of these rare earths in Y_2O_3 were prepared. An internal standard was employed to eliminate run-to-run deviations. One atomic percent gadolinium was incorporated into the Eu, Tb and Dy samples. The residual Dy in the Y_2O_3 was used as the internal standard for Gd. The relative intensities were obtained by comparing the height of the strong lines shown in Figure 2. The minimum detectable relative intensity, based on signal-to-noise ratio of two, was 7×10^{-4}.

Figure 3 shows the relative intensity as a function of concentration for Tb^{3+}, Dy^{3+}, Eu^{3+} and Gd^{3+} in Y_2O_3. A straight line relationship is observed because concentration effects do not occur below 1 to 20 percent for these ions. The minimum detectability of each impurity is indicated in Table I.

TABLE I

MINIMUM CONCENTRATION FOR DETECTION IN Y_2O_3

Rare Earth	Emission Line (cm^{-1})	Minimum Level*
Tb	18400 cm^{-1}	2×10^{-8}
Dy	17500	3×10^{-8}
Eu	17900	1×10^{-6}
Gd	31600	1×10^{-6}

*Expressed as x in $(Y_{1-x}\ Re_x)_2O_3$

The data for Dy^{3+}, Tb^{3+}, and Eu^{3+} all fit very well on a straight line. The reproducibility between runs was better than 5 percent. The data for gadolinium are more scattered than the other rare earths, probably because of a poor choice of internal standard concentration.

Because mechanisms for energy transfer between rare earth ions are inoperative at concentrations below 0-1 atomic percent,[10] spurious results are not to be expected. At higher concentrations energy transfers and absorption may become significant. However, the higher concentrations may be easily detected and analyzed by conventional methods.

OTHER YTTRIUM COMPOUNDS

In view of the marked differences in the Pr^{3+} spectra for the two hosts investigated, it was considered worthwhile to explore other yttrium compounds which might be brighter emitters. A suitable compound should be easily derived from Y_2O_3. Although the garnets generally give brighter fluorescence, they are difficult to synthesize on an analytical sample basis as are other oxide systems. Therefore, we studied a number of rare earth organic systems speculating that an organic-rare earth energy transfer might take place. These included yttrium carbonate, oxalate, acetate, and ethylene diamene cetraacetate (EDTA). These were prepared from the high purity Y_2O_3, which showed a relative Dy^{3+} emission intensity of 3.4×10^{-3}. The salts showed no emission. It was found, however, that if Y(EDTA) was decomposed by heating for one-half hour at 500°C, very bright fluorescense was obtained. The relative Dy intensity increased 50-fold, and Tb^{3+} and Er^{3+} emissions were easily visible with relative intensities of 6.4×10^{-2} and 2×10^{-1} respectively. The increase in the Tb^{3+} and Er^{3+} sensitivity, of course, is not known because they were unobservable in

the original sample; however the Tb^{3+} was certainly below 2×10^{-8}. X-ray diffraction analysis showed that the decomposition product was not Y_2O_3 or any other yttrium compound listed in the 1963 ASTM index of x-ray diffraction patterns. On the basis of color, diffraction pattern and fluorescence brightness the low temperature decomposition product converts to Y_2O_3 between 750° and 1000°C.

SCINTILLATOR APPLICATION

The bright fluorescence under x-irradiation appears to offer advantages in x-ray diffraction over current scintillation materials. Specifically, multiple doping of a synthetic garnet should provide a good match for photomultiplier tubes. In addition to being bright emitters, the garnets are hard, dense, non-hygroscopic materials and $Y_3Al_5O_{12}$ has an absorption constant for 1.54A x-rays approximately three times that of NaI.

To investigate this possibility, we compared the photomultiplier output for undoped $CaWO_4$, with $(Y_{0.99}Tb_{0.01})_2O_3$. The Y_2O_3 gave 70 percent of the response of the $CaWO_4$. Increasing the doping level, adding other dopants, and the use of a garnet host will definitely produce far greater brightness than is now available. Van Uitert[10] has shown more than an order of magnitude increase in the brightness of the 5450Å line of Tb by increasing the concentration to 50 percent in $CaWO_4$. Multiple doping, concentration and lifetime effects are being investigated in our laboratory.

ACKNOWLEDGEMENT

We wish to thank Roger Anderson for his assistance in taking the experimental data.

BIBLIOGRAPHY

[1]J. DeMent, Fluorochemistry, p. 531, 534, and 570.

[2]J. Makovsky, W. Low and S. Yatsiv, Phys. Letters 2, 187 (1962).

[3]W. Low, J. Makovsky and S. Yatsiv, Quantum Electronics III, p. 655, edited by P. Grivet and N. Bloembergen, Columbia University Press, New York (1964).

[4]W. Low, Bulletin Am. Phys. Soc. Series II, 9, 4, 499 (1964).

[5]W. Low, Private Communications.

[6]Sayre, Sancier and Freed, J. Chem. Phys. 23, 2060 (1955).

[7]B.R. Judd, Proc. Roy. Soc. (London) A241, 414 (1957).

[8]E. Carlson and G.H. Dieke, J. Chem. Phys. 29, 229 (1958).

[9]G.H. Dieke and R. Sarup, J. Chem. Phys. 29, 741 (1958).

[10]L.G. Van Uitert and R.R. Soden, J. Chem. Phys. 32, 1161 (1960).

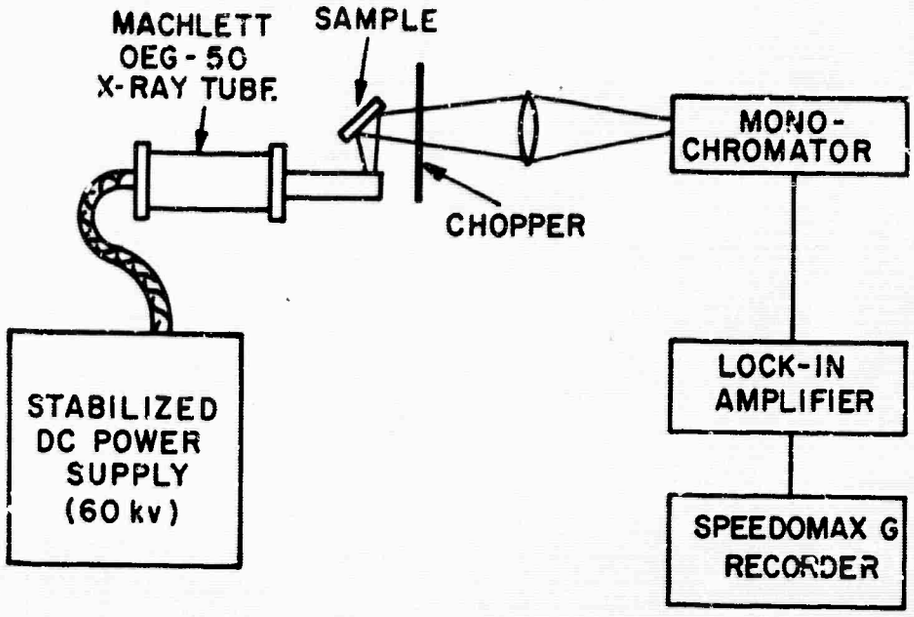

Figure 1. Schematic Representation of Experimental Apparatus

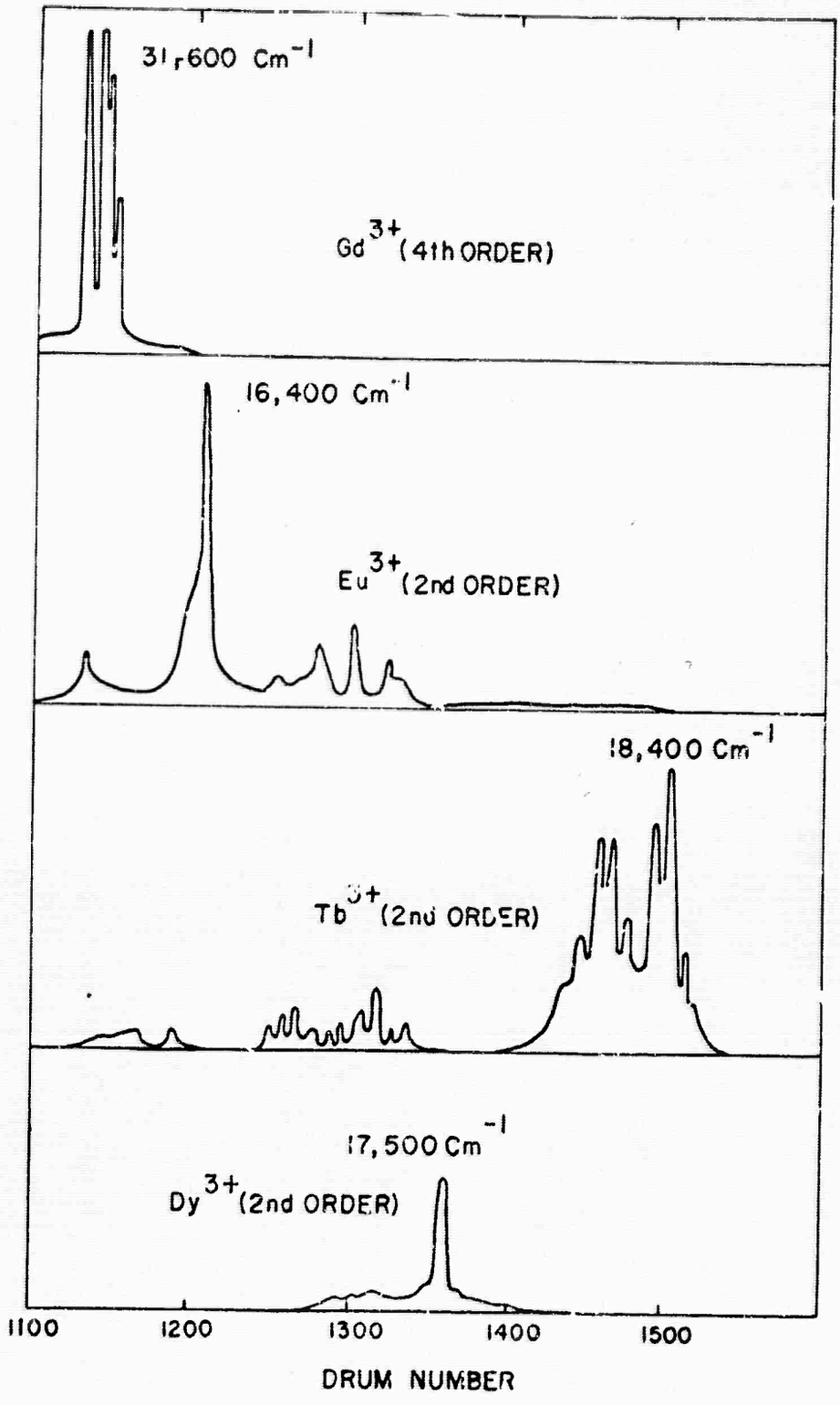

Figure 2. Room Temperature Emission Spectra of 1% Rare Earth in Y_2O_3

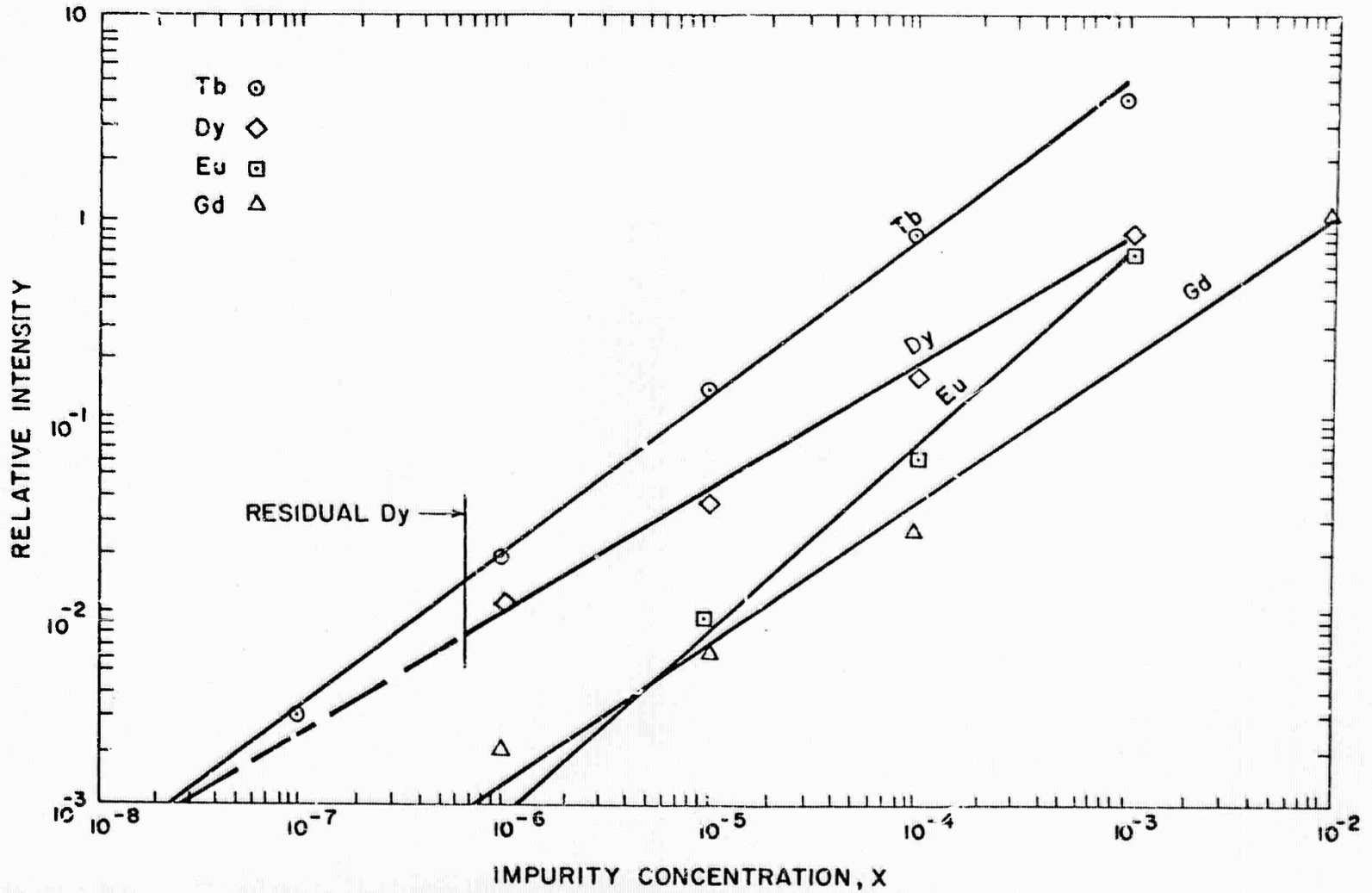

Figure 3. Relative Fluorescent Intensity as a Function of Impurity Concentration, Expressed as x in $(Y_{1-x}Re_x)_2O_3$

APPENDIX III

EMISSION SPECTRA OF RARE EARTHS IN CeO_2 AND ThO_2

APPENDIX III

EMISSION SPECTRA OF RARE EARTHS IN CeO_2 AND ThO_2

The emission spectra of some of the rare earths in CeO_2 and ThO_2 are given in this Appendix. It should be noted that some of the line positions shown here are different from those in the Semiannual Technical Summary Report for the period ending 30 April 1965, due to an error in the previous instrument calibration.

1. EMISSION SPECTRA OF Sm^{3+}

Emission spectra of 0.5At% Sm^{3+} at room temperature are shown in Figure 1. The spectra at 77°K are essentially the same, except for temperature shifts. While these lines are not particularly narrow at room temperature, they are extremely bright with either x-ray or UV excitation. At 77°K the lines are considerably narrowed and the ratio of their brightness change markedly. Figure 2 shows the brightness of the Sm^{3+} content. The brightness is seen to increase slowly up to 1%, whereupon rapid concentration quenching occurs.

The fluorescent lifetime of Sm^{3+} is shown in Figure 3 vs. Sm^{3+} content. Here the lifetime is seen to be inversely proportional to the Sm^{3+} content, from a high of 1.7 msec. to a low of 0.8 msec. At 77°K the lifetime does not vary with concentration, but stays quite constant near 0.70 msec. There are small changes with charge compensation due to the change in site symmetry around the Sm^{3+}, but these are not gross effects.

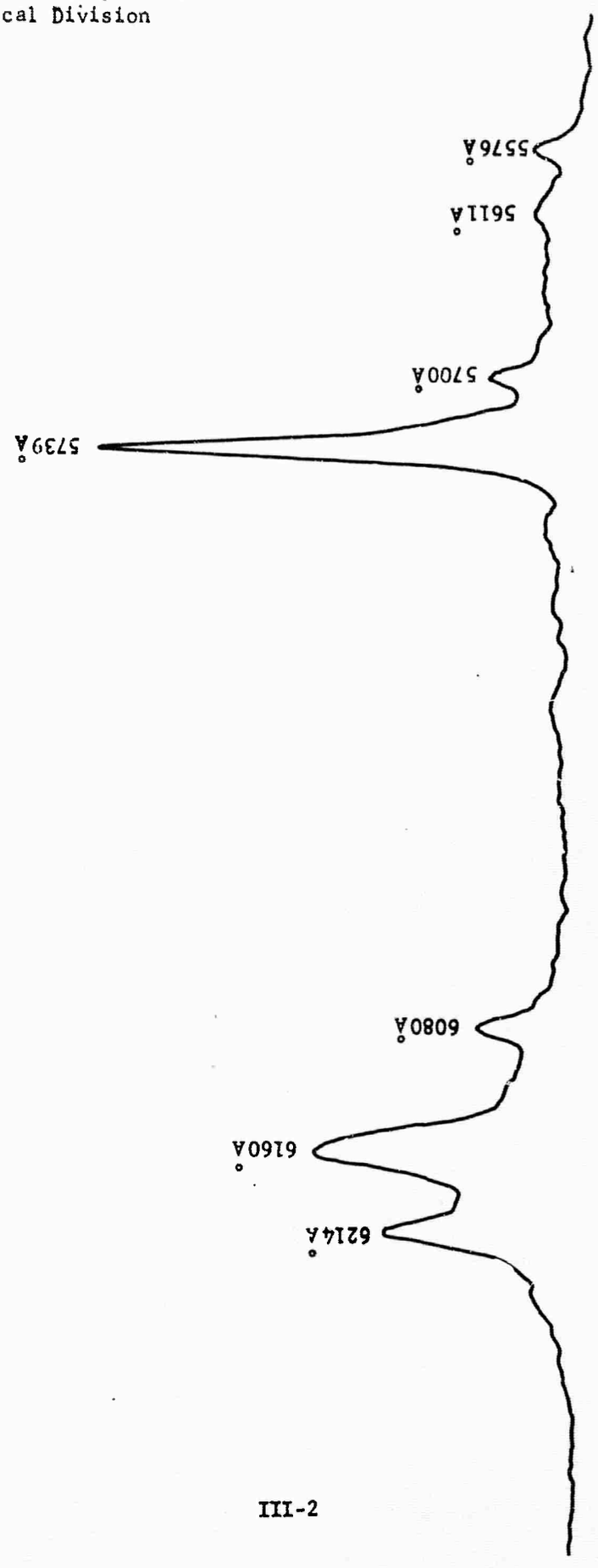

Figure 1. Emission Spectra of CeO_2:0.5% Sm^{3+} (Room Temperature)

TABLE I

SAMARIUM EMISSION LINES

Room Temperature

λ (A ± .5Å)	$\Delta\lambda$ (Å)	Relative Intensity (Corrected for Detector Response)
5576	-	.05
5611	-	.05
5700	-	.005
5739	9.6	1.0
6080	10.2	.16
6160	16.0	.43
6214	13.5	.34

Note: Linewidths have not been corrected for spectral slit width.

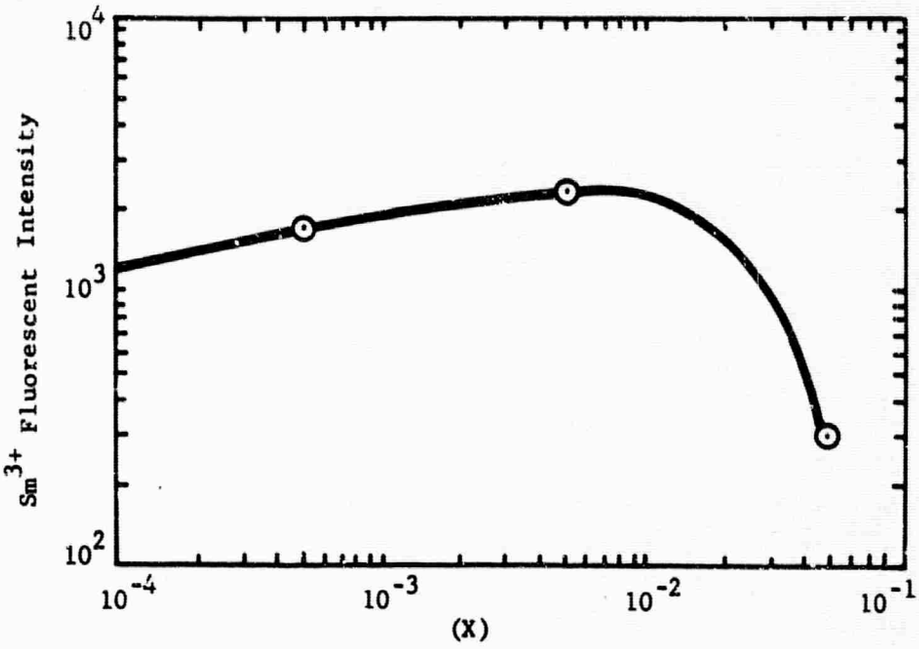

Figure 2. Sm^{3+} Fluorescence Intensity vs. Sm Concentration in $Ce_{1-x}\ Sm_x\ O_2$

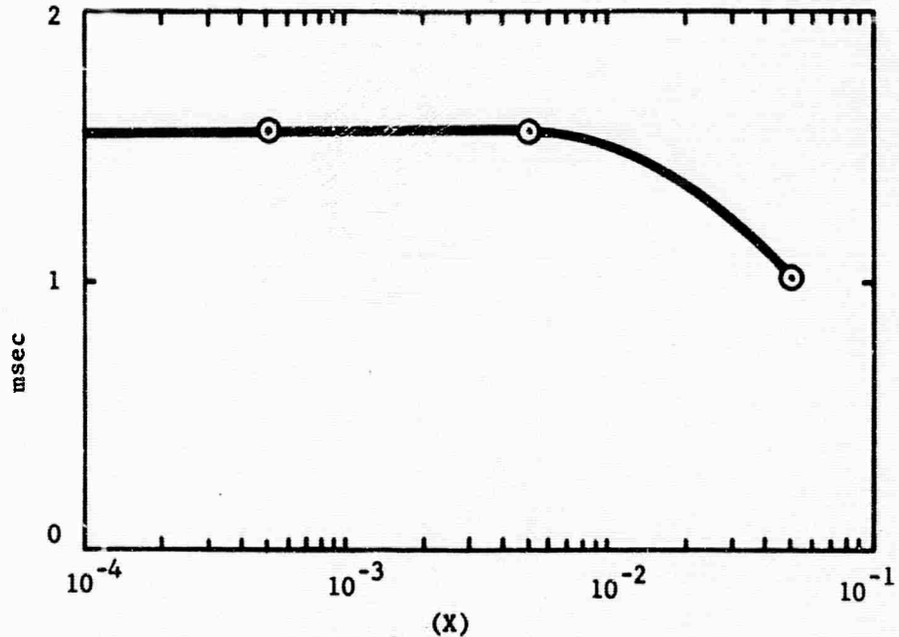

Figure 3. Lifetime Sm^{3+} Fluorescence vs. Sm Concentration in $Ce_{1-x}\ Sm_x\ O_2$

The transmission spectra of several 5% Sm samples was measured in the visible region of the spectrum. However, due to the small thickness (1mm) of sample available at that time, and due to the weak absorption of the samarium lines, no absorptions were seen. The excitation spectra of the 5739Å emission line was also measured in these samples (Figure 4), and again no excitation was found attributable to the weaker lines. The only band responsible for excitation was found from 3870 to 3770Å. There are many other Sm^{3+} levels of equal strength close to this, but they are of lower energies which do not contribute to fluorescence. Since this level lies in the band edge of CeO_2, it appears to be excited by energy transfer from the CeO_2.

a. Sm^{2+}

No emission attributable to Sm^{2+} was observed at either room temperature or 77°K. This was despite deliberate overcompensation with F^{1-} and prolonged x-ray irradiation to reduce Sm^{3+} to Sm^{2+}.

2. EMISSION SPECTRA OF EUROPIUM

a. Eu^{3+}

Emission spectra of 0.5At% Eu^{3+} in CeO_2 at room temperature is shown in Figure 5. The position of these lines, their widths, and relative intensities are given in Table II. The bright lines all originate from the ^5D_o level, but some weak lines from other levels are also seen. At room temperature, the emission between 5800Å and 6600Å is a group of 10 lines. At 77°K, however, there are 15 lines. With 0.5% Eu^{3+} in CeO_2 it would be expected that there should be a large number of europium ions in both trigonal and cubic sites. The larger number of lines then results from further resolving of the spectra, which shows

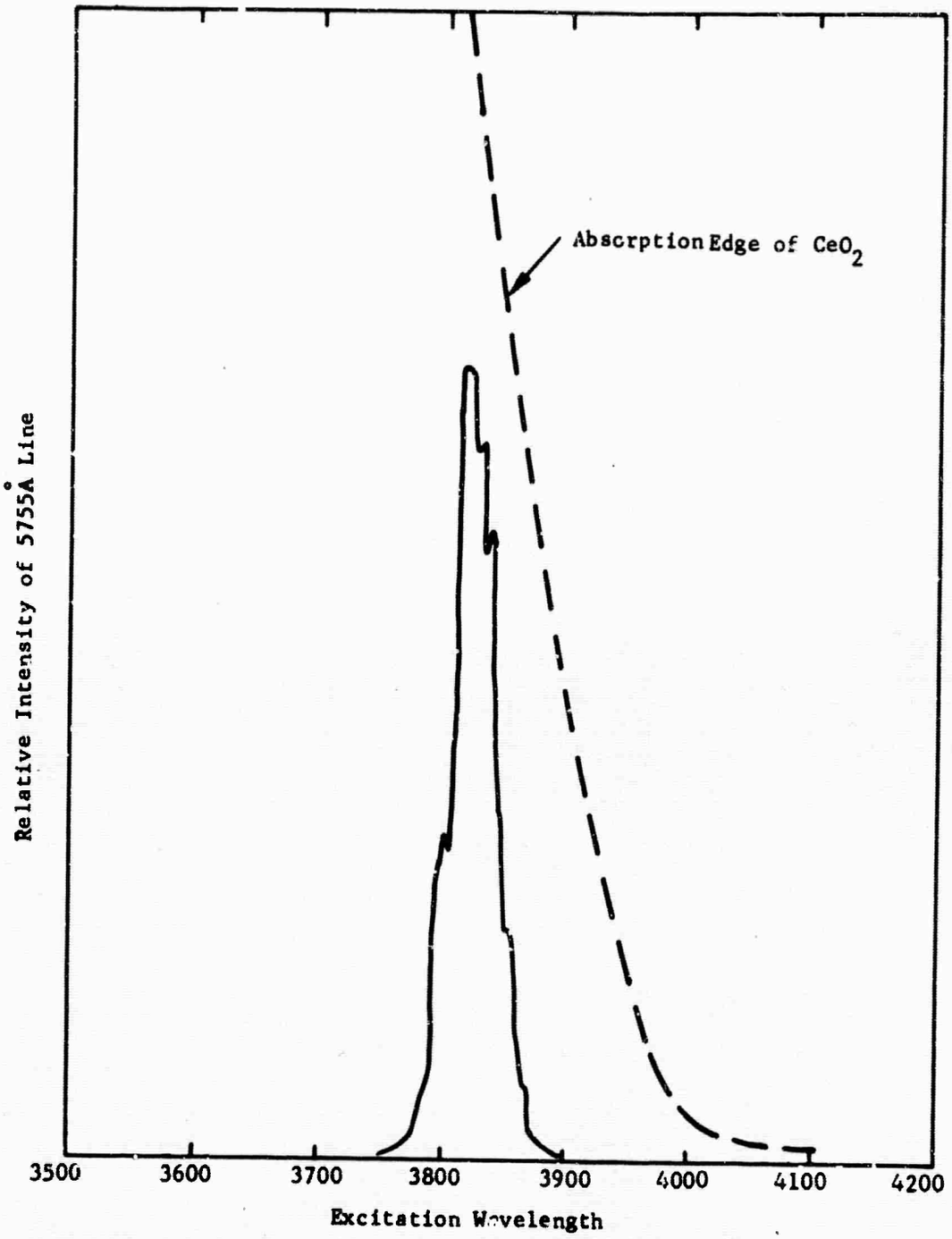

Figure 4. Excitation Spectra of CeO_2: 0.5% Sm^{3+}

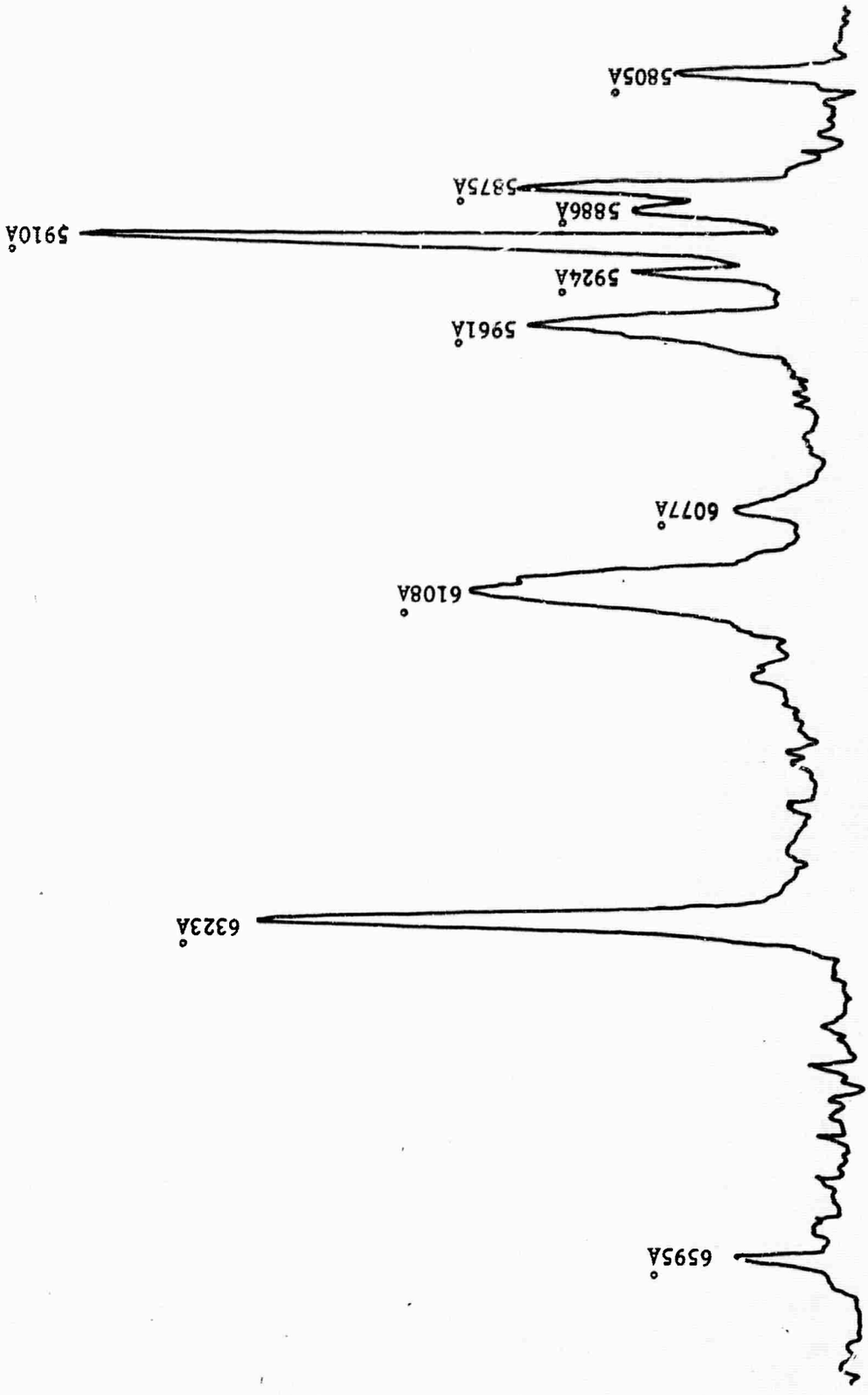

Figure 5. Emission Spectra of CeO_2:0.5% Eu^{3+} (Room Temperature)

TABLE II

EUROPIUM EMISSION LINES

Room Temperature

ν (cm^{-1})	λ (Å ± .5Å)	$\Delta\lambda$ (Å)	Relative Intensity (Corrected for Detector Response)
17,175	5808	2.7	.19
16,968	5875	6.1	.39
16,930	5886	7.65	.27
16,867	5910	4.2Å	1.00
16,816	5924	6.8	.20
16,710	5961	23.5	.27
16,422	6077	10.7	.065
16,287	6108	12.4	.49
15,745	6323	6.7	.97
15,158	6595	5.8	.20

Note: Linewidths have not been corrected for spectral slit width.

the two sites which are partially superimposed at room temperature. The brightness of Eu^{3+} is shown in Figure 6 to be increasing with europium concentration up to at least 5%. A plot of linewidth vs. Eu^{3+} content is given in Figure 7 for the 5910Å line. This shows that there is very little line broadening up to 5% Eu.

3. EMISSION SPECTRA OF ERBIUM

a. Er^{3+}

The visible emission spectra of 5at% Er^{3+} in CeO_2 at room temperature is shown in Figure 8. The room temperature spectrum is characterized by emission in the green. At low temperatures, these levels are partially quenched, and, in addition, emission is seen in the red as observed in calcium tungstate.[1] The wavelengths, linewidths, and relative intensities are summarized in Table III. There are some very narrow lines, all of which terminate quite close to the ground state.

It was not possible to determine the fluorescent lifetime of these lines because they were very weak with optical excitation.

The transmission spectra of Er in CeO_2 show the usual absorptions due to Er^{3+}. Excitation spectra of the 5474Å line (Figure 9), however, do not indicate that these contribute to visible fluorescence. The excitation band for the 5474Å line extends from 3620 to 3700Å, lying in the CeO_2 edge. This level, however, is farther within the edge than Sm^{3+} and Eu^{3+}, and probably largely accounts for the difference in brightness.

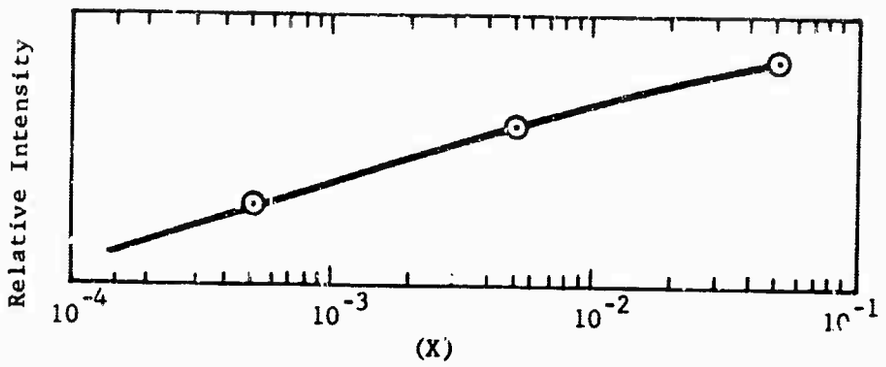

Figure 6. Intensity of 5927Å Line in $Ce_{1-x}Eu_xO_2$

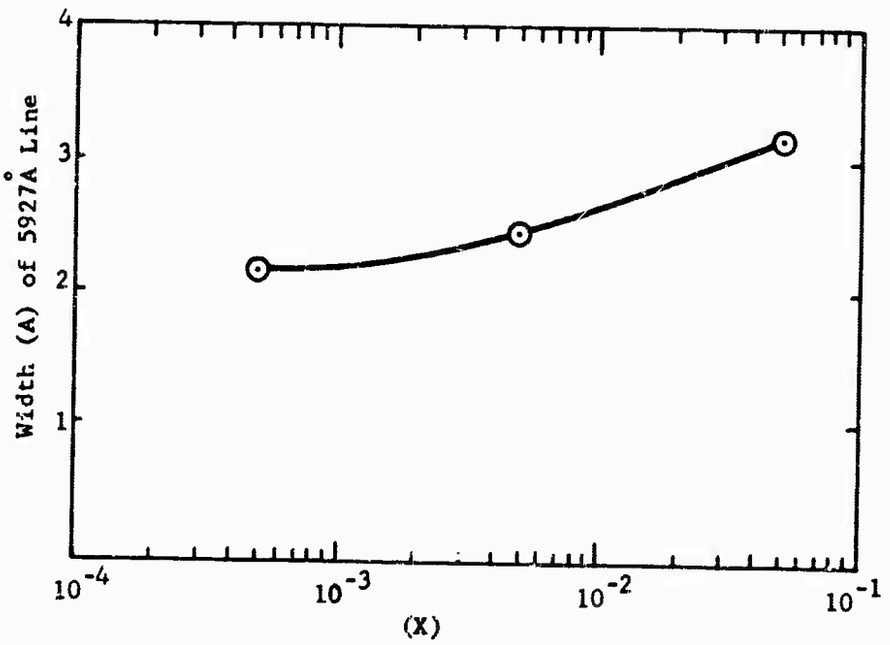

Figure 7. Width of 5927Å Line in $Ce_{1-x}Eu_xO_2$

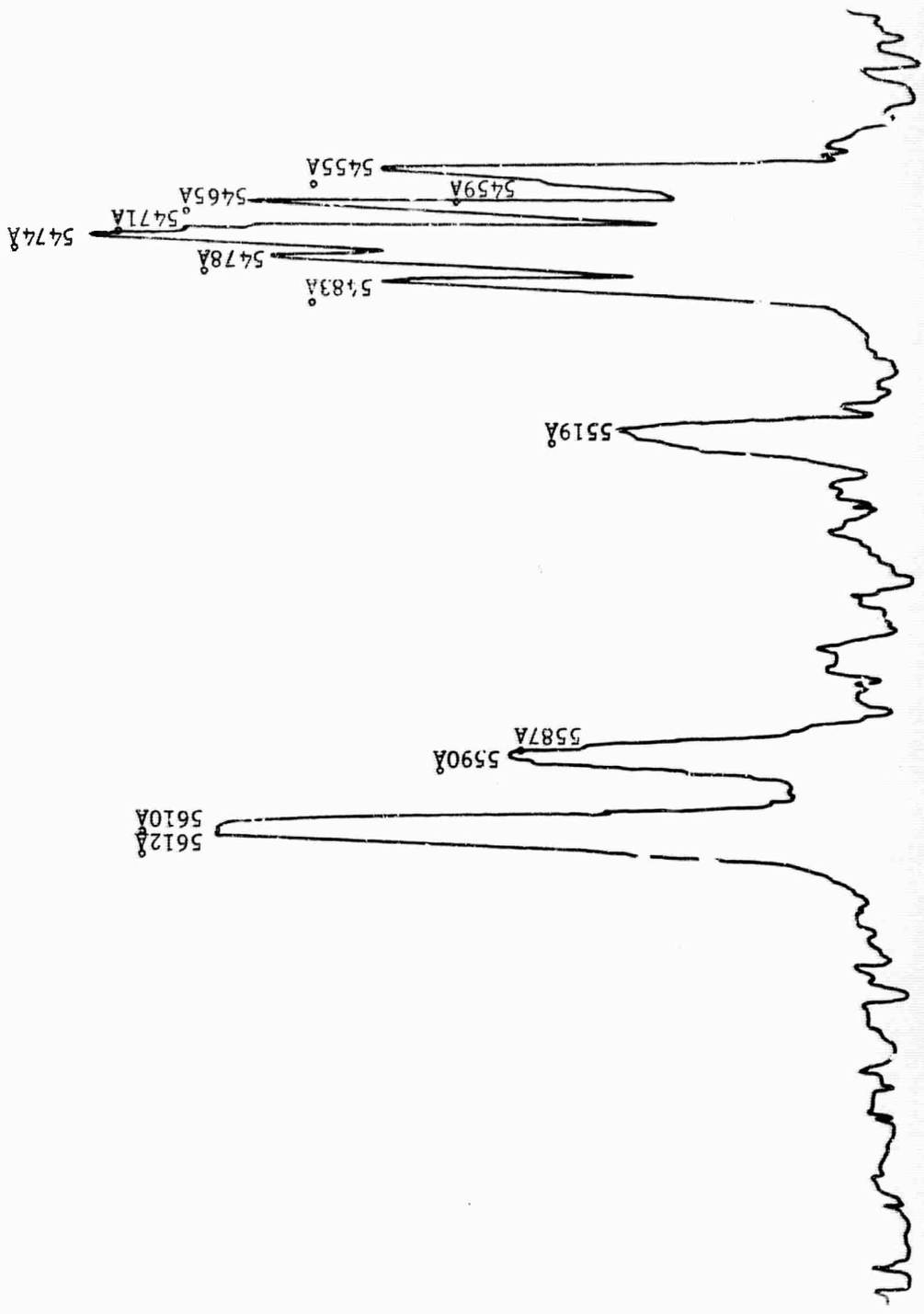

Figure 8. Emission Spectra of CeO_2:0.5% Er^{3+} (Room Temperature)

TABLE III

ERBIUM EMISSION LINES

Room Temperature

λ (Å ± .5Å)	Δλ (Å)	Relative Intensity (Corrected for Detector Response)
5455	2.4	.66
5459	2.3	.50
5465	1.8	.96
5471	2.0	.88
5474	2.2	1.00
5478	1.9	.96
5483	1.9	.72
5519	2.0	.45
5587	3.5	.65
5590	3.0	.65
5610	3.8	.85
5612	3.8	.88

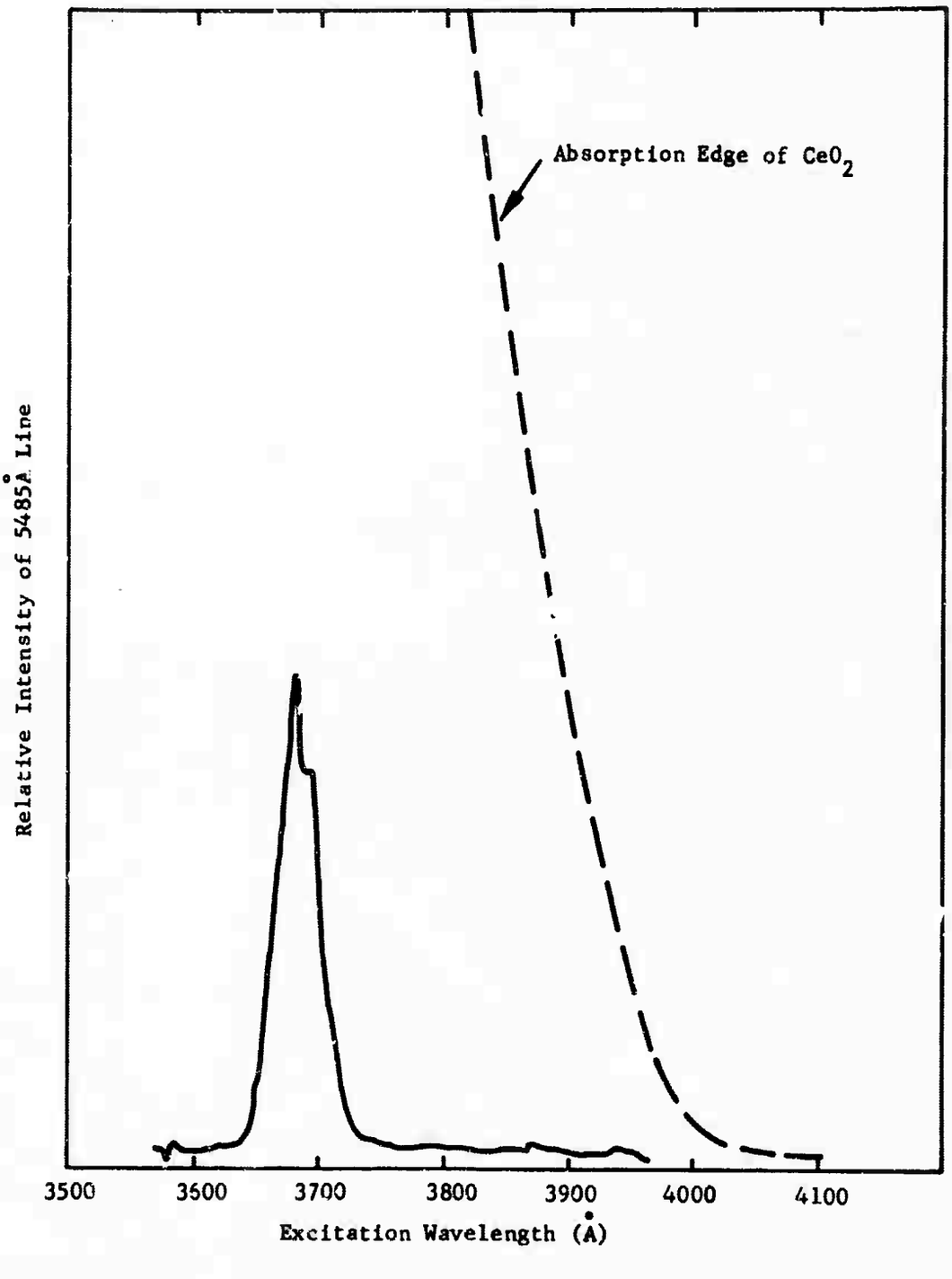

Figure 9. Excitation Spectra of CeO_2: 0.5% Lr^{3+}

What was thought at the time of the Semi-annual Report to be strong infrared emission was found to be a long infrared afterglow in the spark excitation source.

4. EMISSION SPECTRA OF DYSPROSIUM

No visible emission was observed from Dy^{3+} in CeO_2 with x-ray or optical pumping. Transmission measurements indicated that Dy^{3+} was present. However, since the visible emissions originate from levels above the CeO_2 edge, we would not expect emission from them, despite x-ray pumping.

5. EMISSION SPECTRA OF MANGANESE

a. Mn^{2+}

No visible emission attributable to Mn^{2+} was found in CeO_2. Attempts were made to compensate Mn^{2+} by charge compensating with F^{1-} and Ta^{5+} and by vacuum annealing. These attempts were all unsuccessful. The heavily-doped samples were orange in color, like crystals containing Ca^{2+}, and it is possible that the charge compensation ions F^{1-} or Ta^{5+} did not enter the crystal, thereby leaving a color center which would absorb the fluorescence. The vacuum-annealed crystals became black, indicating that Ce^{4+} reduced to Ce^{3+}.

6. EMISSION SPECTRA OF TERBIUM

No visible emission was observed in CeO_2 doped with from 0.05% terbium. The crystals were reddish brown and showed no Tb^{3+} by visual or infrared transmission measurements. Europium was co-doped with terbium to attempt to observe energy transfer to the europium as observed in other compounds.[2] Figure 10 shows the dependence of emission of 0.05% Eu on Tb

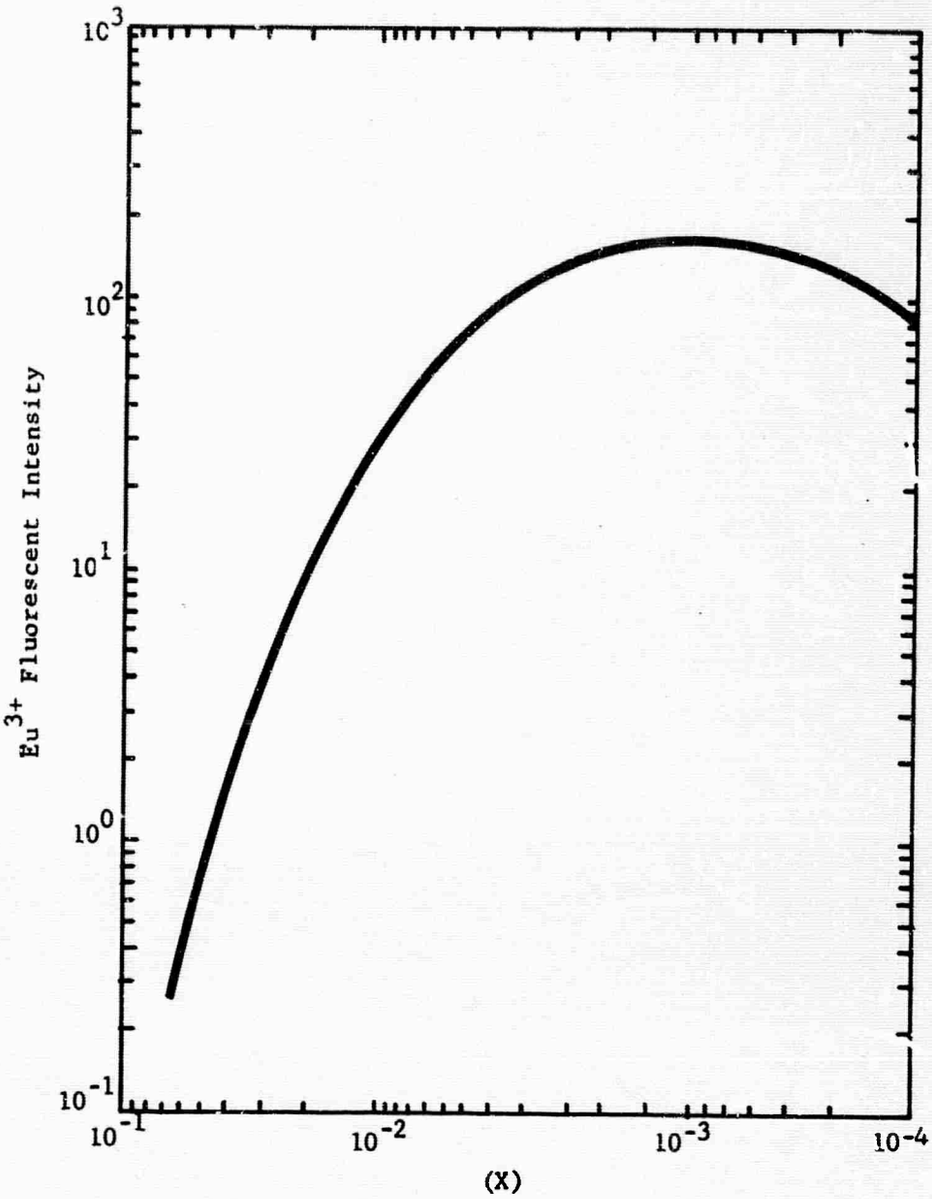

Figure 10. Eu Fluorescence vs. Tb Content in $Ce_{.9995-x}\ Eu_{.0005}\ Tb_x\ O_2$

content. The Eu^{3+} emission increases threefold over a terbium-free sample for the lowest terbium concentration, and then decreases rapidly with terbium content. The increase in brightness with terbium additions indicates that some Tb^{3+} is present. Samples become quite darkly colored at high terbium contents, thus absorbing the Eu^{3+} emission. It is possible, then, that the bulk of the terbium is tetravalent.

A number of crystals containing 5% Tb were vacuum-annealed at 600° for eight hours to attempt to reduce Tb^{4+} to Tb^{3+}. The crystals changed color from reddish brown to pale green; however, no Tb^{3+} was seen.

Unclassified
Security Classification

DOCUMENT CONTROL DATA - R&D

(Security classification of title, body of abstract and indexing annotation must be entered when the overall report is classified)

1. ORIGINATING ACTIVITY *(Corporate author)*
The Perkin-Elmer Corporation
Electro-Optical Division
Norwalk, Connecticut

2a. REPORT SECURITY CLASSIFICATION
Unclassified

2b. GROUP

3. REPORT TITLE
OPTICAL SPECTROPOSCOPY AND CRYSTAL GROWTH OF CeO_2 and ThO_2

4. DESCRIPTIVE NOTES *(Type of report and inclusive dates)*
Yearly Technical Summary Report (for the Period Ending 31 October 1965)

5. AUTHOR(S) *(Last name, first name, initial)*
Linares, Robert C.

6. REPORT DATE	7a. TOTAL NO. OF PAGES	7b. NO. OF REFS
29 November 1965	79	8

8a. CONTRACT OR GRANT NO.	9a. ORIGINATOR'S REPORT NUMBER(S)
Nonr 4660(00)	8197
b. PROJECT NO. ARPA Order No. 306-72	
c. TASK Project Code No. 4730	9b. OTHER REPORT NO(S) *(Any other numbers that may be assigned this report)*.
d.	

10. AVAILABILITY/LIMITATION NOTICES
Qualified requestors may obtain copies of this report from the Defense Documentation Center, Cameron Station Building, Alexandria 14, Virginia

11. SUPPLEMENTARY NOTES	12. SPONSORING MILITARY ACTIVITY
	Department of the Navy, Office of Naval Research, Washington, D.C. 20360

13. ABSTRACT

The optical spectra and crystal growth of CeO_2 and ThO_2 were studied to determine their potential usefulness as laser materials. Crystal growth was carried out by the flux technique. Phase equilibria and solubility determinations were made in order to select a flux for the growth of spectroscopic samples to eventually permit the growth of laser size crystals.

Erbium, terbium, europium, samarium, dysprosium, manganese, and uranium were incorporated into single crystals of CeO_2. Transmission measurements were made on all samples. When samples were observed to fluoresce with x-ray or UV excitation, their emission spectra, excitation spectra, and fluorescent lifetime were studied. The effect of charge compensation on these properties was also studied.

DD FORM 1473 JAN 64

Unclassified
Security Classification